PHYTOCHROME INTERACTING FACTOR 7 moderates the activity of phytochrome A in canopy shade conditions

Mengke Zhou[1*], Andrés Romanowski[2], Karen J. Halliday[1*]

1. Institute for Molecular Plant Sciences, School of Biological Sciences, University of Edinburgh, Edinburgh EH9 3BF, United Kingdom.

2. Timing of Environmental Signaling lab, Molecular Biology Group, Plant Sciences, Wageningen University & Research, Wageningen, The Netherlands.

ORCID IDs: 0000-0003-1043-2766 (MK. Z); 0000-0003-0737-2408 (A.R.); 0000-0003-0467-104X (K.J.H.).

*Corresponding authors:
Mengke Zhou and Karen J. Halliday
Institute for Molecular Plant Sciences, School of Biological Sciences, University of Edinburgh, Edinburgh EH9 3BF, United Kingdom
+44-0131-651-9083
mengke.zhou@ed.ac.uk
karen.halliday@ed.ac.uk

ABSTRACT

In nature, plants perceive and respond to complex vegetative environments through the phytochrome (phy) photoreceptor-signaling system. The canopy adaptation strategy, elicited by phyA, together with the shade avoidance syndrome, regulated by phyB, enables plants to adapt to diverse forms of vegetation shade. The phyA High Irradiance Response (HIR) mode, which involves photocycle-coupled nuclear shuttling, is essential for sensing sustained far-red rich conditions typical of canopy or occlusive shade. Our research identifies PHYTOCHROME INTERACTION FACTOR 7 (PIF7) as a key regulator of phyA function. We show that PIF7ox effectively suppresses phyA action. Under persistent shade, PIF7 and phyA both accumulate and interact within nuclear photobodies, with binding mediated by the C-terminal domain of PIF7 and the PAS-PAS domain of phyA. PIF7 also interacts with FHY1 and FHL transport facilitators, thereby interfering with phyA cytosolic-nuclear shuttling. This coordinated molecular targeting by PIF7 constitutes an effective strategy for modulating phyA function under shaded conditions.

INTRODUCTION

Light sensing is fundamental for plant adaptation and survival in vegetative shade. This is particularly important during seedling establishment, a stage when plants are most vulnerable. Plants have evolved distinct developmental strategies to cope with different types of shade that are prevalent in nature. The light receptor phytochrome B (phyB), is able to detect FR-rich light from neighboring plants and elicit the Shade Avoidance Syndrome (SAS), which induces elongation of seedling hypocotyls, repositions leaves to improve light capture, and triggers early flowering (*1,2*). Under persistent canopy shade, plants adopt alternative strategies, such as the phyA-mediated Canopy Adaptation Strategy (CAS), which suppresses hypocotyl elongation and conserves resources, optimizing growth when shade is unyielding (*3*). As vegetative habitats can change considerably through a season, the ability to adjust photoreceptor activity offers adaptive flexibility, ensuring successful seedling establishment and progression through the life cycle. In Arabidopsis, phytochromes A-E, form a family of photoreceptors that principally absorb light in the red (R) and far-red (FR) regions of the spectrum (*4*). Absorption of R photoconverts phytochrome into its active Pfr form, while FR photoconverts Pfr to the inactive Pr conformer. When activated phytochromes move from the cytosol to the nucleus where they aggregate in sub-nuclear photobodies to perform a range of functions (*5,6*). While all phytochromes possess similar photosensory properties, they fall into two classes based on their distinct modes of action. Phytochromes B-E, which operate in the low fluence response (LFR) mode, are activated by R and deactivated by FR light. Consequently, in FR-rich vegetation shade environments, these phytochromes are less active (*4,7*). A key distinction of phyA is that it is activated by FR-rich light through its high irradiance response (HIR) mode of action (*7*). This property arises partly from its photobiology and partly from the shuttling mechanism that concentrates phyA in the nucleus (*8*). PhyA lacks a nuclear localization signal and primarily relies on the proteins FHY1/FHL to facilitate its transport into the nucleus. These proteins specifically recognize phyA-Pfr and transport it to the nucleus, where it is converted into phyA-Pr, allowing FHY1/FHL to dissociate and be recycled to the cytoplasm for further

shuttling (*8-10*). Nuclear located phyA regulates a number of processes, including expression of target genes, through association with transcription factors such as PHYTOCHROME INTERACTING FACTORS (PIFS) and ELONGATED HYPOCOTYL 5 (HY5) (*11*). The central role of FHY1/FHL shuttling in the phyA HIR, identifies this mechanism as a potential target for modifying phyA action and the adaptive response (*8*). Indeed, HY5 has been reported to be involved in negative-feedback regulation of phyA signaling through repressing FHY1/FHL expression (*11*). Here, HY5 directly interacts with the DNA-binding regions of FAR-RED ELONGATED HYPOCOTYLS 3 (FHY3) and FAR-RED IMPAIRED RESPONSE 1 (FAR1) to prevent their transcriptional activation of FHY1/FHL.

PIF transcription factors are well-studied negative regulators of phytochrome signaling. They function by directly binding G/PBE-boxes in the promoters of their target genes (*12*). In Arabidopsis, there are eight PIFs (PIF1, PIF2/PIL1-PIF8), each with an active phytochrome B (APB) domain that facilitates their interaction with phyB. Only PIF1 and PIF3 contain an active phytochrome A (APA) domain, which directly binds the C-terminus of phyA, comprising two Period-Arnt-SIM (PAS) and a histidine kinase-related (HKRD) domain (*13*). In FR light, phyA directly interacts with PIF1 and PIF3, triggering their proteolytic destruction and/or sequestration from target promoters (*13,14*). Although PIF4, PIF5, PIF8 and PIF7 lack an APA domain, they have been shown to control aspects of phyA signaling (*15-17*). Interestingly, levels of PIF8 protein are boosted by phyA. In darkness, CONSTITUTIVE PHOTOMORPHOGENESIS 1 (COP1) promotes PIF8 protein degradation through the 26S proteasome, thereby reducing its abundance. Conversely, under FR light, phyA inhibition of COP1 stabilizes the PIF8 protein, forming a negative feedback loop that limits phyA action (*15*).

Notably, PIF7, a close homologue of PIF8, is a potent regulator of SAS. In unshaded conditions, PIF7 interacts with active phyB (Pfr) through its APB domain, and both proteins localize to sub-nuclear photobodies. This interaction prevents PIF7 from binding to the promoters of target genes, effectively inhibiting PIF7-regulated gene expression (*18,19*). Under shade conditions, the deactivation of phyB releases PIF7 from this repression, leading to the activation of shade-responsive genes and triggering the physiological SAS response (*20,21*). Furthermore, exposure to shade triggers the dephosphorylation and nuclear accumulation of PIF7, processes that enhance the activation of SAS (*20*). Given its strong promotory role in SAS, it is notable that PIF7 has recently been demonstrated to increase *PHYA* transcript abundance, an action that could potentially limit SAS. This PIF7 action can be inhibited by *PHYA UTR ANTISENSE RNA (PUAR),* which binds to PIF7 and prevents its interaction with *PHYA'*s 5' UTR, thereby reducing *PHYA* transcript levels (*17*). Collectively, this research underscores the importance of PIF7 as a key agent in executing and moderating the molecular response to shade.

Here, we show that PIF7 modulates phyA signaling under vegetative shade by controlling phyA subcellular localization and activity. PIF7 overexpression (PIF7ox) abolishes phyA-mediated suppression of seedling hypocotyl elongation under persistent shade. Under these conditions, PIF7 and phyA co-localize in nuclear

105 photobodies and interact directly via the PIF7 prion-like domain and the phyA C-terminus. Additionally, our
106 data shows that PIF7 governs phyA subcellular localization by modulating FHY1/FHL-dependent nuclear
107 import. These insights clarify how PIF7 effectively restricts both the nuclear transport and signaling
108 activities of phyA, illuminating the intricate molecular mechanisms at play.

109 **RESULTS**

110 **PIF7ox blocks phyA action**

111 PIF7, which functions downstream of phyB, also shares significant sequence similarity with PIF8, a
112 regulator of phyA responses. This similarity led us to investigate the potential genetic interaction between
113 PIF7 and phyA. To achieve this, we measured the hypocotyl length of 6-day-old seedlings grown under two
114 regimes: 8-hour light (PAR = 85 ± 5 μmol m^{-2} s^{-1}): 16-hour dark cycle (WL) at 22°C, or identical conditions
115 with continuous far-red (FR) light supplied through the photoperiod (WLFR) (Fig. 1A). This second regime
116 was designed to simulate persistent moderate shade, delivering a red:far-red (R:FR) ratio of 0.2 and Pfr/Ptot
117 of 0.27 (fig. S1 and table S1). In all experiments, supplementary FR light was applied from one day after
118 germination to align with the optimal period for phytochrome A (phyA) action during seedling development
119 (*3,22*). As expected, exposure to WLFR inhibited hypocotyl elongation in wild-type (WT, Col-0) seedlings,
120 whereas *phyA-211* mutants instead showed enhanced elongation in WLFR (Fig. 1B). This pronounced
121 elongation in *phyA-211* reflects the loss of phyA-mediated repression of SAS, which is predominantly
122 initiated by phyB inactivation under WLFR conditions (*22,23*) The phyAox line exhibited a constitutively
123 short hypocotyl, which was further reduced under WLFR (Fig. 1B). Together, these results confirm that our
124 simulated shade growth regime effectively activates phyA-dependent inhibition of hypocotyl elongation and
125 robustly counteracts SAS-associated growth.

126 We also found that similar to phyAox, the loss-of-function alleles *pif7-1* and *pif7-2* exhibited slightly shorter
127 hypocotyls than the WT while maintaining responsiveness to WLFR (Fig. 1, B and C). These phenotypic
128 effects were abolished by the *phyA-211* mutation, as observed in the *pif7-1;phyA-211* double mutant.
129 Consistent with the established role of PIF7 in promoting the phyB-mediated SAS, in WLFR *pif7-1* reduced
130 hypocotyl elongation in the *phyA-211* background (*24,25*). In comparison, hypocotyls of *p35S::PIF7-*
131 *FLASH* (PIF7ox) seedlings, which have 3-fold (WL) change than WT higher expression (fig. S2), were
132 significantly elongated under WL, with WLFR inducing a further increase in elongation (Fig. 1, B and C).
133 While PIF7ox and PIF7ox;*phyA-211* exhibited nearly identical hypocotyl responses. Our findings, therefore,
134 provide genetic evidence linking PIF7 and phyA. This relationship is particularly evident in PIF7ox
135 seedlings, which display exaggerated SAS-associated elongation and a complete loss of the WLFR-induced
136 phyA response (Fig. 1, B and C). The data collectively suggests a mechanism in which PIF7 participates in
137 a cross-regulatory interaction between phyB and phyA.

138 Given the capacity of PIF7ox to inhibit phyA activity, we next examined the possibility of functional
139 redundancy with other PIFs. As anticipated, PIF8ox also lacked WLFR-mediated growth inhibition, but
140 PIF3ox, PIF4ox and PIF5ox all retained this response (fig. S3, A and B) (*15*). Our data therefore illustrate
141 that even though PIF3, PIF4 and PIF5 have been implicated in *PHYA* regulation and signaling, their roles
142 are functionally distinct from those of PIF7 and PIF8 (*16,26,27*). We found the hypocotyl lengths of *pif8-1*
143 to be comparable to WT, while *pif8-1* slightly reduced the impact of *phyA-211* on hypocotyl elongation in
144 WLFR, as observed in *pif8-1*;*phyA-211* (fig. S3C). Further, PIF8ox;*phyA-211* hypocotyls were more
145 elongated than PIF8ox, indicating that while PIF8ox suppresses the phyA-dependent response, it does not
146 completely eliminate it. These findings are consistent with the reported role of PIF8 as a negative regulator
147 of phyA signaling (*15*). However, our data also showed the genetic interaction with *phyA-211* differs
148 between PIF8ox and PIF7ox. Whereas *phyA-211* is epistatic to PIF8ox, the relationship is reversed for
149 PIF7ox, which is epistatic to *phyA-211* (Fig. 1, B and fig. S3C). The difference in epistasis for PIF7 likely
150 reflects its dual role in phyA- and phyB-mediated signaling pathways. However, with respect to phyA
151 signaling, we wanted to determine whether PIF7 has an analogous role to PIF8, or if it operates through a
152 different mechanism.

153 **PIF7 moderates phyA protein abundance**

154 Previous studies have demonstrated that *PHYA* expression is strongly induced by shade and that PIF7
155 increases *PHYA* transcript abundance through binding to the *PHYA* 5′ UTR (*3*,17). Consistent with these
156 findings, we observed that under an 8L:16D photoperiod, sampling one hour before dusk (ZT7), WLFR
157 enhanced *PHYA* expression in WT seedlings, whereas this response was attenuated in the *pif7-1* mutant (Fig.
158 1D). In comparison, PIF7ox exhibited elevated *PHYA* levels in control conditions, which were further
159 enhanced in WLFR.

160 Immunoblot analysis with an antibody against native phyA revealed consistently low phyA levels under WL
161 across all genotypes, reflecting the well-established light lability of phyA and its degradation upon white
162 light exposure (*3,28*) (Fig. 1, E and F). Indeed, we also found that PIF7ox had minimal effect on
163 *pPHYA::PHYA-nLUC* (phyA-nLUC) activity through a WL photoperiod, where reporter levels gradually
164 decline over the course of the day (Fig. 1G) (*3*). In contrast, under WLFR, phyA protein levels were elevated
165 in WT, further increased in PIF7ox, and reduced in *pif7-1*, closely reflecting the corresponding patterns of
166 *PHYA* gene expression (Fig. 1, D to F). We also observed higher levels of daytime phyA-nLUC in WLFR,
167 which was notably elevated by PIF7ox (Fig. 1G) (*3*). Thus, our findings demonstrate that under WLFR
168 conditions, PIF7 regulates *PHYA* expression and the abundance of phyA protein. However, despite
169 accumulating significantly higher levels of phyA under WLFR, PIF7ox seedlings fail to elicit a phyA
170 response. This indicates that the regulatory effect of PIF7ox on phyA activity does not stem from changes
171 in phyA abundance.

172 To examine the *in vivo* dynamics of PIF7 under our experimental conditions, we generated *pPIF7::PIF7-*
173 *nLUC* (PIF7-nLUC) lines. We discovered that PIF7-nLUC exhibits rhythmic patterns, with higher levels
174 during the day compared to the night (fig. S4A). WLFR boosted daytime levels of PIF7-nLUC levels, with
175 the *phyA-211* mutation elevating PIF7-nLUC toward the end of the period, especially in WLFR (fig. S4B).
176 Therefore, our data indicated that similar to phyA, WLFR increases the abundance of PIF7, and that phyA
177 plays a minor role in reducing PIF7 production toward the end of the photoperiod.

178 **PIF7 can interact with phyA in nuclear photobodies**

179 To establish whether PIF7 and phyA are found in the same cellular location we analyzed transgenic lines
180 expressing *pPHYA::PHYA*-sGFP (phyA-GFP) and *p35S:GFP-PIF7* (PIF7-GFP). Consistent with earlier
181 studies, we found that under WL, PIF7-GFP and phyA-GFP were predominantly in the cytosol, while
182 exposure to WLFR enhanced their nuclear localization (fig. S5)(*20,29,30*) Previously, PIF7 was shown to
183 form sub-nuclear photobodies, or speckles, in response to red light (*18*). Similarly, we observed nuclear PIF7
184 photobodies in WL and discovered that PIF7 also formed photobodies under WLFR (fig. S6). As phyA-GFP
185 locates to photobodies in WLFR, we reasoned that PIF7 and phyA may co-localize in these sub-nuclear foci
186 (fig. S6). To investigate this, we employed the *p35S::PIF7-sfGFP* (PIF7-GFP) and *p35S::PHYA-RFP*
187 (phyA-RFP) constructs which were transiently expressed in *N. benthamiana* leaves. After exposure to
188 WLFR, we observed co-localization of PIF7-GFP and phyA-RFP in nuclei and in photobodies (Fig. 2A).
189 Quantitative fluorescence measurements along a nuclear transect, intersecting two photobodies, confirmed
190 this co-localization (Fig. 2A).

191 Next, we created split bimolecular fluorescence complementation (BiFC) constructs *p35S::PIF7-nYFP*
192 (PIF7-nYFP) and *p35S::PHYA-cYFP* (phyA-cYFP*)*, to test whether PIF7 and phyA physically interact *in*
193 *vivo*. Initially, we analyzed the *p35S::EGFP* control, which was detected across cytosolic and nuclear
194 compartments under both WL and WLFR (Fig. 2B). In contrast, our BiFC assays with PIF7-nYFP and phyA-
195 cYFP exhibited strong signals in the nucleus and in sub-nuclear foci following exposure to WLFR. Notably,
196 these signals were absent in control lines expressing *p35S::PIF7-nYFP* and *p35S::EV-cYFP.* The findings
197 suggest that PIF7 and phyA can indeed interact under WLFR conditions (Fig. 2B).

198 To gain further evidence for this interaction we also generated split nanoLUC (nLUC) luciferase reporter
199 constructs, *p35S::PIF7-lgbitnLUC* (PIF7-lgbit) and *p35S::PHYA-smbitnLUC* (phyA-smbit), with
200 *p35S::PHYB-smbitnLUC* (phyB-smbit) and *p35S::PHYA-nLUC* (phyA-nLUC) as controls (Fig. 2C). As
201 expected, the phyA-nLUC control emitted a strong signal in WLFR compared to WL, as WLFR typically
202 enhances phyA abundance (*3*). Conversely, the PIF7-lgbit+phyB-smbit control had a strong signal in WL
203 which diminished in WLFR, consistent with the known light conditional interaction between PIF7 and phyB
204 (*18*). The negative controls (phyA-smbit + phyB-smbit) had low signals in both conditions. In the WL regime,
205 the signal from PIF7-lgbit + phyA-smbit was low, similar to that of the negative control, whereas in WLFR,

206 the signal was strong, confirming the WLFR-specific PIF7-phyA interaction. Additionally, using an
207 antibody against native phyA, we demonstrated co-immunoprecipitation of phyA with PIF7ox, in WLFR
208 but not WL conditions (Fig. 2D). Thus, our data provides evidence that PIF7 and phyA directly interact
209 within photobodies after exposure to WLFR, which promotes their respective nuclear accumulation (*20,31*).

210 Interestingly, our data illustrates that PIF7-GFP forms photobodies in both WL and WLFR, yet phyA
211 photobodies are only detected in our WLFR regime (fig. S6). We therefore reasoned that PIF7 may play a
212 role in phyA photobody formation under WLFR. In support of this notion, we found that in WLFR, phyA-
213 GFP photobodies were not detectable in *pif7-1* but were more abundant in the PIF7ox line (Fig. 2E). It
214 therefore appears that PIF7 may be required for phyA to photobody formation in WLFR.

215 **The PIF7 C-terminus interacts with the phyA PAS-PAS domain**

216 Earlier work demonstrated that phyA binds directly with PIF1 and PIF3. The phyA C-terminal domain is
217 known to be important for this interaction, as is the active phyA-binding domains (APA) of PIF1 and
218 PIF3(*13,26*). To identify PHYA regions that required for the molecular interaction we utilized *p35S::PIF7-*
219 *nYFP* (PIF7-nYFP) and *p35S::PHYA-cYFP* (phyA-cYFP) split YFP assay, creating truncated PHYA
220 constructs as follows: C-terminal (PHYA-C), comprising HINGE (H), PAS-PAS DOMAIN (PAS), and
221 HISTIDINE KINASE RELATED DOMAIN (HKRD) regions [*H+PAS+HKRD-cYFP*], PHYA-C1
222 [*PAS+HKRD-cYFP*], PHYA-P [*PAS-cYFP*], and PHYA-H [*HKRD-cYFP*] (Fig. 3A). As before, the
223 *p35S::EGFP* control exhibited non-specific cellular localization pattern in WL and WLFR (Fig. 2B and Fig,
224 3A). In contrast we obtained WLFR-specific nuclear fluorescence signals for PIF7-nYFP and the full-length
225 phyA-cYFP control, as well as the truncated PHYA-C, PHYA-C1, and PHYA-P constructs. No signal was
226 observed for PHYA-H and the negative EV control. The strong signal detected for PHYA-P, which includes
227 PAS-PAS domain motifs, highlights the significance of this molecular region in facilitating the interaction
228 with PIF7.

229 To identify the region of PIF7 that mediated the interaction with phyA, we generated PIF7-N which contains
230 the ACTIVE PHYTOCHROME BINDING domain [*PIF7-N-nYFP*], PIF7-B, containing the BASIC
231 HELIX-LOOP-HELIX motif [*PIF7-B-nYFP*], and PIF7-C [*PIF7-C-nYFP*] which contains a polyQ-rich,
232 prion-like domain (Fig. 3B and fig. S7). Interestingly we found that only the PIF7 full length control and
233 PIF7-C gave nuclear fluorescence in WLFR. Thus, our data point to the C-terminal region of PIF7 as being
234 important for its interaction with phyA.

235 **PIF7ox blocks phyA regulation of target genes**

236 To further interrogate the mechanism through which PIF7 inhibits phyA action we initially tested whether
237 PIF7 alters the expression of genes (*CHS, BIN2, FHY3, FHY1*, *FHL* and *IAA29)* known to be directly
238 regulated by phyA (Fig. 4A) (*32,33*). As determined by qPCR all the genes, except *IAA29*, were upregulated

239 in WT in WLFR conditions, otherwise, the expression patterns fell into two categories. In WLFR conditions,
240 *CHS, BIN2,* and *FHY3* exhibited decreased expression in both *phyA-211* and PIF7ox, while their expression
241 was increased in *pif7-1*. This gene set is upregulated by phyA in WLFR, and their expression is repressed
242 by PIF7. On the other hand, *FHY1, FHYL* and *IAA29* form a group that are upregulated in *phyA-211* and
243 PIF7ox, and for *FHY1* and *FHYL*, expression is lowered in *pif7-1*. These genes are downregulated by phyA
244 in WLFR, and their expression is promoted by PIF7. The common factor for all these genes is that phyA and
245 PIF7 exert opposing control of their regulation, particularly in WLFR. We then sought to establish if the
246 antagonistic action of PIF7 was mediated through direct repression of phyA at target gene promoters. Here
247 we performed chromatin immunoprecipitation (ChIP) using a native phyA antibody, and qPCR using to
248 detect phyA enrichment at *CHS, FHY1*, and *FHL* promoters. For all three genes we found WLFR stimulated
249 phyA enrichment at promoter regions sequences containing G-box motifs (two in *CHS*), but not in G-box-
250 free regions (control, coding region) (Fig. 4, B and C). This enrichment was eliminated in the presence of
251 PIF7ox, suggesting the interaction between PIF7 and phyA is able to block phyA regulation of target genes.

252 **PIF7 interacts with FHY1 and FHL**

253 In FR-rich conditions FHY1 and FHL play a pivotal role in facilitating the transport of phyA into the nucleus,
254 and they have been linked to the regulation of phyA target genes (*9,10,23*). Notably, FHY1 has been
255 implicated in the recruitment of phyA to the *CHS* promoter through its direct binding to HY5 or PIF3 (*34*).
256 The importance of FHY1 and FHL in our WLFR conditions is evident in the *fhy1-3;fhl-1* double mutant
257 hypocotyl response which is phenotypically similar to *phyA-211* (fig. S8). Consequently, we aimed to
258 determine whether PIF7 interacts with FHY1 and FHL in addition to phyA. Using the *N. benthamiana*
259 transient expression system, we recorded BiFC nuclear interactions between *p35S::PIF7-nYFP (PIF7-nYFP)*
260 and the *p35S::FHY1-cYFP (FHY1-cYFP), p35S::FHL-cYFP (FHL-cYFP)* constructs under WLFR
261 conditions, but not with the *35S::EV-cYFP* control (Fig. 5A. In our split nLUC assay we also observed PIF7-
262 lgbit interactions with FHY1-smbit and FHL-smbit, but not the negative control, under WLFR (Fig. 5B). It
263 is worth noting that in this assay, the interaction signal strength between the shuttle proteins and PIF7 was
264 weaker than that observed between PIF7 and phyA (Fg. 5B). However, we were able to verify these
265 interactions through co-immunoprecipitation using *p35S::FHY1/FHL-nLUC* (FHY1/FHL-nLUC) and
266 *p35S::PIF7-sfGFP* (PIF7-GFP) in *N. benthamiana* (Fig. 5C and fig. S9). As our data shows that PIF7 can
267 interact with phyA, FHY1 and FHL, we postulated that these proteins may form a complex under inductive
268 WLFR conditions. Lending some support for this hypothesis, we found that when FHY1-YFP or FHL-YFP
269 are co-expressed with PIF7-GFP and phyA-RFP in *N. benthamiana* leaves, these constructs localize to the
270 same nuclear regions under WLFR (Fig. 5, D and E).

271 Interestingly, we also found the expression of *ARABIDOPSIS SUMO PROTEASE 1 (ASP1)*, a crucial factor
272 in SUMOylation and the maintenance of FHY1 levels under FR light conditions to be PIF7-dependent (*35*).

273 In WT, *ASP1* levels are increased by WLFR, a response that is further amplified by *pif7-1* and suppressed
274 by PIF7ox (fig. S10). Thus, *ASP1* may provide a route for PIF7 to indirectly regulate FHY1.

275 Since PIF7 is able to interact with FHY1 and FHL we were interested to establish if PIF7 affected phyA
276 nuclear shuttling. To address this question, we measured the proportion of cells with nuclear vs cytosolic
277 phyA-GFP signals in the *pif7-1* and PIF7ox backgrounds. In WL, we found this ratio to be similar in all
278 genotypes (Fig. 5, F and G). Whereas in WLFR, we recorded a higher proportion of nuclear phyA-GFP in
279 WT, that was even greater in the *pif7-1* mutant, and diminished in PIF7ox (Fig. 5, F and G). Given that
280 PIF7ox has elevated phyA levels (Fig. 1, E to G), we reasoned that this could potentially skew the proportion
281 of nuclear to cytosolic phyA. However, the observation that *pif7-1* has a slightly higher nuclear fraction of
282 phyA compared to WT, despite having lower phyA levels, suggests that PIF7 may indeed influence the
283 cellular distribution of phyA (Fig. 5, F and G). To verify our results, we performed immunoblot assays that
284 differentiated between nuclear and cytosolic fractions. This method yielded qualitatively similar results
285 showing increased nuclear phyA in *pif7-1* and predominately cytosolic PHYA in PIF7ox under WLFR (fig.
286 S11). Thus, it is possible that PIF7 binding to FHY1 and FHL, may partially disrupt the nuclear transport of
287 phyA.

288 **phyA-NLS inhibits PIF7ox action**

289 To determine if PIF7 primarily acts by sequestering phyA or whether the PIF7 interactions with FHY1/FHL
290 are also important, we employed *p35S::PHYA-tagRFP:terRbcS* (phyAox) and *pPHYA::PHYA-sGFP-NLS*
291 (phyA-NLS), where phyA is constitutively nuclear (fig. S12) (*30*). In line with earlier findings, under our
292 experimental conditions, phyAox and phyA-NLS restore the elongated *phyA* mutant hypocotyl phenotype
293 to WT length (Fig. 6A). We hypothesized that if PIF7 regulation of phyA was solely due to its interaction
294 with phyA, then PIF7ox should diminish the function of phyAox and phyA-NLS through this mechanism
295 (*30*). However, while this is the case for phyAox, we found phyA-NLS exhibits strong epistasis over PIF7ox
296 for control of hypocotyl length. Similarly, for *CHS* and *IAA29* gene expression under WLFR conditions,
297 PIF7ox suppressed the effects of phyAox, while conversely, phyA-NLS diminished the impact of PIF7ox
298 on *CHS* and *IAA29* (Fig. 6, B and C). These findings are not attributable to variations in phyA levels, as
299 immunoblot analyses show that under WLFR conditions, phyA levels are slightly reduced in phyA-NLS
300 compared to phyAox (fig. S13). Consequently, the potent effects of PIF7ox on phyA action, are unlikely to
301 arise solely from the PIF7-phyA interaction.

302 Previous research demonstrated that phyA-NLS completely restores phyA control of hypocotyl growth in
303 *fhy1-3;fhl-1 and phyA-211;fhy1-3;fhl-1*, indicating that phyA-NLS can bypass the requirement for nuclear
304 shuttling (*36*) . The effectiveness of PIF7ox on phyAox, which utilizes FHY1/FHL, and not phyA-NLS,
305 suggests that the interaction between PIF7 and FHY1/FHL may be required to suppress phyA action. One
306 possibility is that PIF7 interacts with phyA-FHY1/FHL complexes soon after their nuclear entry and before

307 the complexes disassemble. Interestingly, our fluorescence data illustrate that PIF7-GFP, phyA-RFP and
308 FHY1-YFP or FHY1-YFP co-localize within both the nucleus and photobodies under WLFR conditions
309 (Fig. 5, D and E) (*9*). Collectively, our data indicates that PIF7 forms inactive complexes with phyA and
310 FHY1/FHL, which appear to dampen shuttling and to impede phyA signaling.

311 **DISCUSSION**

312 PIF7 is known to be a phyB-regulated transcription factor, with a key role in mediating shade-avoidance
313 responses (*18*). This study further reveals that PIF7 is instrumental in controlling phyA signaling, positioning
314 it at the nexus of phyA and phyB pathways. PIF7 operates in persistent shade, conditions that elevate phyA
315 abundance and promote its nuclear accumulation through the FHY1- and FHL-mediated nuclear shuttling
316 mechanism (*9,10*). Our findings demonstrate that PIF7 effectively modulates phyA signaling through direct
317 interactions with phyA as well as with the transport proteins FHY1 and FHL. This regulatory function of
318 PIF7, which occurs within photobodies, directly interferes with phyA-mediated gene expression control.

319 PIF7 is particularly active in FR-rich shade, which triggers its dephosphorylation, increases its nuclear
320 abundance (fig. S5) (*20*). Since continuous shade also stimulates phyA activity, it creates favorable
321 conditions for interactions between PIF7 and phyA. Indeed, our results demonstrate that PIF7 and phyA
322 physically interact, as evidenced by BiFC (PIF7-nYFP + phyA-cYFP) and split nLUC (PIF7-lgbit and phyA-
323 smbit) transient expression assays, alongside *in vivo* co-immunoprecipitation of PIF7ox and phyA (Fig. 2,
324 B to D). Previously, PIF1 and PIF3 were shown to interact with phyA through their respective Active
325 Phytochrome A-binding (APA) domains (*15,37*). This binding is known to facilitate the proteolysis of PIF1
326 and PIF3, and to inhibit the activity of PIF3 by isolating it from target promoters (*15,37,38*). PIF7, however,
327 lacks an APA domain, yet it is still capable of binding to phyA. Our data reveal that this interaction is
328 facilitated through the PAS domain of phyA and the C-terminal region of PIF7. Additionally, our ChIP-
329 qPCR assays demonstrate that PIF7 moderates phyA activity by inhibiting its ability to bind to target
330 promoters (Fig. 4, B and C). For the genes *CHS*, *FHY3*, and *BIN2*, which are activated by phyA in WLFR,
331 and for *FHY1*, *FHL*, *IAA29*, which are repressed by phyA, PIF7 counteracts the effects of phyA. Previously,
332 our research demonstrated that PIF7 interacts with and suppresses the transcriptional activity of
333 ANGUSTIFOLIA 3 (AN3), a promoter of leaf cell proliferation (*40*). In this context, PIF7 operates by
334 sequestering and substituting for AN3 at target promoters. These findings suggest that PIF7 can assemble
335 distinct nuclear complexes to modulate the activity of diverse transcriptional regulators.

336 The proteins FHY1 and FHL are integral to phyA function as they facilitate its nuclear translocation, and
337 FHY1 is proposed to regulate a subset of target genes in concert with phyA (*32,34*). Through the use of BiFc,
338 split nanoLUC and co-immunoprecipitation assays, we have shown that in addition to phyA, PIF7 also
339 interacts with FHY1 and FHL under WLFR (Fig.5, A to C). Under shade conditions, phyA nuclear import
340 is a highly dynamic process that depends on the efficient recycling of FHY1/FHL after dissociation of the
341 nuclear phyA–shuttle protein complex (*8,10, 41,42*). Sequestration of FHY1 and/or FHL by PIF7 could
342 therefore restrict their availability and mobility, thereby reducing their capacity to transport phyA into the

343 nucleus. Consistent with this model, our data reveals an altered cytosolic to nuclear distribution of phyA in
344 hypocotyl epidermal cells of *pif7-1* and PIF7ox (Fig. 5, F and G). Thus, PIF7 appears to affect more than
345 one aspect of phyA function.

346 In white or red light PIF7 is known to colocalize with phyB in nuclear photobodies (*18,19*). Formation of
347 phyB-PIF7 nuclear condensates is thought to limit the availability of PIF7 for transcriptional regulation
348 (*18,19,43,44*). Conversely, exposure to low R:FR light deactivates phyB, triggering photobody dissolution
349 and releasing PIF7 to bind DNA and mediate chromatin modifications. This study reveals that under
350 persistent shade conditions, PIF7 relocates to distinct photobodies where it co-localizes with phyA and the
351 shuttle proteins FHY1 and FHL (Fig. 5, D and E).

352 PIF7 is unique amongst PIF proteins as it contains a prion-like domain with a central polyQ stretch of 17
353 consecutive glutamine residues (fig S7). Prion-like domains typically comprise low-complexity or
354 intrinsically disordered regions that facilitate protein condensation and liquid-liquid phase separation (LLPS).
355 Indeed, PIF7 has been shown to form condensates with LLPS characteristics *in vitro*, which is proposed to
356 facilitate the formation of PIF7-phyB photobodies (*19*). Substituting polyQ with polyA diminishes the
357 capacity of PIF7 to form photobodies, highlighting the importance of polyQ in this process. It is therefore
358 possible that PIF7 also fulfils a similar function in facilitating the formation of PIF7-phyA photobodies.
359 Across organisms, the spatial organization of biomolecules into distinct cellular locations is essential for
360 enabling specialized functions (*45*). Our data suggests that in persistent shade PIF7 may function to sequester
361 phyA along with FHY1 and FHL, thus limiting their operational effectiveness.

362 We also sought to determine whether the interaction between PIF7 and phyA represents the primary
363 mechanism by which PIF7 regulates phyA signaling. If this were the case, we reasoned that PIF7ox should
364 suppress the effects of both phyAox and phyA-NLS. However, while PIF7ox effectively counteracts the
365 impact of phyAox, it fails to suppress the effects of phyA-NLS on hypocotyl elongation and *CHS* and *IAA29*
366 expression (Fig. 6, A to C). Because phyAox depends on nuclear shuttling for its activity, whereas phyA-
367 NLS is constitutively nuclear and bypasses the FHY1/FHL-mediated transport pathway, these findings
368 suggest that PIF7 interaction with FHY1/FHL, in addition to phyA itself, may be required to attenuate phyA
369 signaling. Therefore, it appears that simultaneously targeting both the receptor and its transport machinery
370 enables PIF7 to effectively suppress this dynamic signaling pathway.

371 In summary, our study outlines the central role PIF7 plays in regulating phyA activity (Fig. 6 D). Its direct
372 binding to phyA, and the FHY1/FHL transporters, likely represents a rapid, energy-efficient, and highly
373 effective way to stem phyA action. The compartmentalization of phyA and FHY1/FHL into PIF7
374 photobodies constitutes a dynamic regulatory mechanism that responds to changes in environmental light
375 quality. This subcellular partitioning enables PIF7 to drive hypocotyl elongation while simultaneously
376 reducing the suppressive influence of phyA. Since the modulation of PIF7 by phyB is well-established, our

377 findings position PIF7 at the molecular intersection of phyB and phyA, underscoring its pivotal role in
378 adjusting phyA activity to promote SAS elongation under vegetative shade (*19*).

379 **METHODS**

380 **Plant material and growth conditions**

381 The wild-type of *Arabidopsis thaliana* seedlings are Columbia-0 (Col-0). The *pif7-1*, *pif7-2* (*46*), *pif8-1*,
382 *pif8-2* mutants, and the construction of *pif8-1;phyA-211*, PIF8ox*;phyA-211* and PIF8ox (*15*), PIF7ox-
383 FLASH(*47*), *p35S::GFP-PIF7* (*20*), *p35S::PIF3-LUC* (*48*), *p35S::PIF5-HA*, *p35S::PIF4-LUC* (*16*),
384 *pPHYA::PHYA-sGFP, pPHYA::PHYA-sGFP-NLS* (*30*), and *pPHYA::PHYA-nanoLUC-3×FLAG-10×His*
385 (phyA-nLUC) (*3*) have been described previously. The *phyA-211* mutant was obtained from NASC
386 collection. *pPIF7::PIF7-nanoLUC-3×FLAG-10×His* (PIF7-nLUC) (Basta) were transformed into the *pif7-*
387 *1* background. The phyA-GFP-NLS*;pif7-1* and PIF7ox;phyA-GFP-NLS, *pif7-1*;*phyA-211* and
388 PIF7ox;*phyA-211* lines were generated by genetic crossing method. Likewise, the *pif7-1;*phyA-nLUC,
389 PIF7ox;phyA-nLUC, PIF7-nLUC;*pif7-1*;*phyA-211* lines were made through genetic crossing. All the cross
390 lines were verified using PCR or sequencing.

391 For the hypocotyl growth experiments seeds were first sterilized and then re-suspended in 0.1% (w/v) agar
392 and stored in darkness at 4 ºC for 3 d to stratify. Following this, seeds were individually sown onto plates
393 containing half-strength Murashige and Skoog basal salts mixture (Duchefa Biochemie, Haarlem,
394 Netherlands) dissolved in 1% (w/v) agar (1/2 MS media; pH 5.8). The plates were then transferred to Percival
395 I30BLL growth chambers at 22 ºC (Plant Climatics, Wertingen, Germany). To promote germination seeds
396 were exposed to a 4 h period of white light (WL) (85±5 µmol m^{-2} s^{-1}), and then darkness for 20 h, before
397 transferring to experimental photoperiods. For all experiments, seedlings were grown under short day
398 (8L:16D) conditions in either WL or WL with supplementary FR (WLFR) to provide a R:FR ratio of 0.20,
399 PAR=85±5 µmol m^{-2} s^{-1}(fig. S1 and Table S1). The condition data collected through L1-180 Spectrometer
400 (LI-COR®).

401 **RNA extraction and qPCR**

402 For RNA extraction seedlings (n = 36 ± 5 seedling numbers), were harvested at Zeitgeber time 7 (ZT), one
403 hour before dusk. Total RNA was extracted using a phenol-based method (*40*), 300 µL RNA extraction
404 buffer (PH=8.0) was added to each sample, followed by 300 µL 1:1 acidic phenol: chloroform. The
405 supernatant was separated from the pellet by centrifuging for 15 minutes at 13,000 rpm under 4 ºC. Up to
406 300 µL of the supernatant was transferred to collection tubes with 240 µL isopropanol and 30 µL 3 M sodium
407 acetate. Samples were precipitated at -80 ºC for 15 minutes, then centrifuged for 30 minutes at 13,000 rpm.
408 Pellets were washed with 300 µL of 70% ethanol and then suspended in nuclease-free water and stored at -
409 80 ºC. Complementary DNA (cDNA) synthesis was performed using the qScript cDNA SuperMix (Quanta
410 Biosciences) as described by the manufacturer. A Lightcycler 480 system (Roche) was employed for qPCR,

411 with 10 μL reactions that incorporated the SYBR Green Master Mix (Roche). The qPCR primers are shown
412 in Supplementary (Table S2). Results were analyzed using Light Cycler 480 (Roche) followed by the ΔΔCt
413 method.

414 **Hypocotyl measurements and statistical analysis**

415 Images of hypocotyls were taken after 6 days of growth. Hypocotyl length was analyzed using ImageJ
416 (https://imagej.nih.gov/ij/). Data was analyzed by Excel and GraphPad Prism 10. Data are presented as mean
417 values ± s.e.m. A Two-way ANOVA test was used to obtain statistical significance (α=0.05); the Tukey's
418 HSD posthoc test for multiple comparisons. Levels that are not significantly different are marked with the
419 same letter. Representative images from three independent replicates are shown in all figs.

420 **Construct assembly**

421 The full-length CDS of *PHYA* and nanoLUC tag (*nanoLUC-3×FLAG-10×His*; NL3F10H) have been
422 described previously (*3*). The CDS of *PIF7* were synthesized by the GeneArt Gene Synthesis service
423 (Invitrogen, MA, USA). The split nanoLUC tags were made by splitting nanoLUC to lgbit (158 aa) and
424 smbit (11 aa). Mobius Assembly was used to insert the constructs into a mUAV plasmid (L0, CamR) with
425 *AraI* restriction site and plasmid assembly was performed and subsequently verified by the Edinburgh
426 Genome Foundry (*49*). The full-length CDS of *FHY1* and *FHL* parts were amplified with Q5 High-Fidelity
427 DNA polymerase (New England Biolabs, MA, USA) from the Col-0 cDNA by gene-specific primers. The
428 *PHYA-C*, *PHYA-C1*, *PHYA-P*, *PHYA-H*, *PIF7-N*, *PIF7-B* and *PIF7-C* part cloned on the CDS region of
429 *PHYA* and *PIF7* (L0 parts). These parts were assembled into a mUAV plasmid and sequenced by Source
430 Bioscience (Cambridge, UK). All L0 parts will assemble in pMAP B L1 (KamR) vector with *BsaI* restriction
431 site. All the constructs for the tobacco (*Nicotiana benthamiana*) assay used a CaMV35S promoter, which is
432 synthesized by the GeneArt Gene Synthesis service (Invitrogen, MA, USA).

433 To construct *pEXP601-pPIF7::PIF7-nanoLUC-3×FLAG-10×His*, a 2740 bp genomic fragment was
434 generated, encompassing the PIF7 promoter region (1015 bp), 5'UTR (161 bp), and 1564 bp ORF, excluding
435 the stop codon of exon 6 of the AT5G61270.1 gene model. This fragment was PCR-amplified using specific
436 primers with Phusion High-Fidelity DNA Polymerase (NEB, M0530S). The resulting amplicon was
437 subsequently recombined into pDONR221 using BP II clonase (Invitrogen, 12535029), and its sequence
438 verified by Sanger sequencing (Genepool, Edinburgh Genomics, Edinburgh, UK). The genomic regions
439 were then recombined into *pGWB601:nanoLUC-3×FLAG-10×Hiss* using LR Clonase (Invitrogen) (*50*).
440 The final construct was transformed into Agrobacterium AGL1. Primers used for construct assembly are
441 listed in Supplementary (Table S3).

442 **Transient Expression Assay**

443 For this assay, constructs were transferred into the Agrobacterium AGL1 strain and cultured at 28 ºC for two
444 days, before infiltration into 4-week-old *Nicotiana benthamiana* leaves with P19. The transient expression
445 solution contained 10 mM MES buffer (pH 5.6), 10 mM $MgCl_2$ and 200 mM aceto-syringone. Following
446 infiltration plants were grown for 3 days in short day (8L:16D, at 22 ºC) conditions in either WL or WLFR
447 to provide a R:FR ratio of 0.20. Samples were analyzed at ZT7 on day 3.

448 **Confocal Imaging, Colocalization, and BiFC**

449 Images of GFP, YFP and RFP fluorescence were obtained with a Leica confocal micro-scope (Leica SP8)
450 using 488 nm and 552 nm lasers. For BiFC and co-localization assay all images were taken at ZT7 on day 3
451 after WL/WLFR treatments. The co-localization signals were analyzed by LAS X Office 1.4.7.2982 and
452 plotted by GraphPad Prism 10. *pPHYA::PHYA-sGFP(NLS)*, phyA-GFP;*pif7-1*, phyA-GFP;PIF7ox and
453 *p35S::GFP-PIF7* transgenic lines images were taken at ZT7 within 30 minutes after 6 days of WL/WLFR
454 treatments.

455 The Nuclear and cytosolic signals were quantified from 50 cells in the mid-hypocotyl region within a 20 ×
456 1.36 objective lens. Nucleus and cytoplasmic signals were quantified after eliminating background
457 interference by Image J. Then plotted in GraphPad Prism 10 (*32*). Imaging experiments were comprised of
458 three biological replicates, with 6 seedlings per replicate.

459 **Immunoblot Analysis and Co-immunoprecipitation Assays**

460 Each sample comprised 0.5 g of Arabidopsis seedling tissue, harvested on day 6 at ZT7. The seedlings
461 grounded into fine powder in liquid nitrogen and then homogenized in double the volume of pre-cooled lysis
462 buffer which contained 1× Protease inhibitor (Sigma-Aldrich, P9599) and 1× HALT-Phosphatase inhibitor
463 (Thermo Scientific) (125 mM Tris-HCl (pH 7.5); 0.25mM EDTA (pH 7.5), 150 mM NaCl, 5% glycerol,
464 0.1% Triton X-100, 0.5% NP-40). Then mixture samples were centrifuged at 12,000 rpm for 10 mins at 4
465 ºC and then transferred to lysate mix with 1× SDS loading buffer (containing 0.1 M DTT) at a 1:1 volume
466 ratio. Samples were incubated at 80 ºC for 10 mins, followed by a centrifugation step, before western blotting.

467 For Co-immunoprecipitation, the different light-treated Arabidopsis seedlings(0.5-1g) or *Nicotiana*
468 *benthamiana* leaves (2-3 g) were ground to a fine powder in liquid nitrogen and then homogenized in double
469 the volume of pre-cooled lysis buffer which contained 1× Protease inhibitor (Sigma-Aldrich, P9599) and 1×
470 HALT-Phosphatase inhibitor (Thermo Scientific) (125 mM Tris-HCl (pH 7.5); 0.25mM EDTA (pH 7.5),
471 150 mM NaCl, 5% glycerol, 0.1% Triton X-100, 0.5% NP-40) after lysis we kept this mixture on ice for 30
472 minutes and centrifuge 10 minutes with 12,000 rpm. The supernate was filtered twice through two layers of
473 Mira cloth (Merck Millipore). After 100 ul supernatant, consisting of total protein extracts as input, and the
474 other supernatant were incubated with Protein A/G beads (MCE Magnetic Agarose) for 1 h at 4 °C to remove
475 adventitious binding proteins. After incubating with Protein A/G beads, moved beads from supernatant by
476 Magnetic Separation Rack. Then anti-FLAG/His beads (Anti-FLAG M2 agarose gel Sigma-Aldrich, Cat.No.

477 A2220; Anti-His Magnetic Beads, Cat. 209, MCE) were added into treated protein extracts and kept
478 overnight at 4 ºC (Before adding the antibody-beads, used wash buffer wash beads 3 times). The
479 antibody/protein complex was washed with wash buffer (125 mM Tris-HCl [pH 7.5]; 0.25mM EDTA [pH
480 7.5], 150 mM NaCl, 5% glycerol, 0.1 % Triton X-100) 5 times. Then, 50 µL of 1× SDS loading buffer were
481 added to each sample and incubated at 80 ºC for 8 mins.

482 To detect native phyA protein, an anti-Phytochrome A antibody (PHYTOAB, PHY1907) was used at
483 1:1,000. To detect the PIF7ox-FLASH and *p35S::FHY1/FHL-nanoLUC × 3FLAG× 10His* an anti-FLAG
484 M2 antibody (Sigma-Aldrich, F1804) was used at 1:2,000. To detect the *p35S::PIF7-sfGFP* an anti-GFP
485 anti-body (Roche, ab290) was used at 1:3,000. Anti-RPN6 antibody (Agrisera, AS121858) was used at
486 1:3,000 as internal control. Secondary antibodies (1:3,000, anti-mouse IgG (cell signaling, 7076s); 1:4,000
487 Goat anti-rabbit-IgG (Abcam, AB6013) were used for the ECL Prime Western Blotting System. The signals
488 were detected by Azure 300 Imager with ECL prime western blotting detection reagents (Cytiva, RPN2232).

489 **NanoLUC and split nanoLUC assays**

490 NanoLUC bioluminescence assay was conducted as previously described (*3*). Single Arabidopsis seedlings
491 were grown in individual wells, within a 96-well plate, each containing 200 µl 1/2 MS media. Plates were
492 sealed with cling film and placed under 8L:16D (WL) for 6 days. Before imaging, 50 µl of 1:50 water
493 dilution of Nano-Glo buffer (Promega, Nano-Glo®Luciferase Assay) was added to the seedlings in each
494 well. Plates were sealed and moved to experimental light conditions. Bioluminescence was recorded every
495 hour (for 1.5 s) for several days using the TriStar2 LB942 multimode microplate reader (Berthold
496 Technologies, Germany). In Fig. 1G, the data were analyzed by averaging individual seedling measurements
497 and then calculating the fold change relative to the ZT0 data for each biological replicate. Subsequently, the
498 results were plotted using GraphPad Prism 10. A total of 9 biological replicates were conducted, with each
499 replicate comprising at least 6 seedlings. In fig. S4, the data was analyzed by BioDare2 software, applying
500 amp&baseline detrending and normalization steps, before plotting in GraphPad Prism 10 (*51*)

501 The split nanoLUC assay utilized the *N. benthamiana* transient expression system described above.
502 Following WL/WLFR treatments for 3 days, 1cm x 1cm leaf samples (n =12) were transferred to 96 wells
503 plates containing 100 µl diluted (1:50) Nano-Glo for imaging with a plate reader. The data analyzed by Excel
504 and GraphPad Prism 10. Experiments repeated at least 3 times.

505 **Chromatin Immunoprecipitation (ChIP)-qPCR**

506 We employed ChIP-qPCR methods described previously (*52*). For each sample 0.5-1 g of tissue was
507 extracted from 6-day old seedlings at ZT7. Cross-linking was induced with 1% formaldehyde under vacuum
508 infiltration for 15 mins (up to -70 kPa), then 2.5 ml of 2 M glycine was added to quench crosslinking. DNA
509 was fragmented into an average size of ~150 bp in Diagenode BioRuptor Plus, (30 cycles of high power 30s
510 ON / 30s OFF). Anti- PHYA antibody (PHYTOAB, PHY1907,1:300) incubated with protein A/G beads

511 (MCE Magnetic Agarose) in 4 ºC overnight. And the following day, samples were incubated with protein
512 A/G bead/PHYA antibody complex for 6 hours at 4 ºC. DNA was extracted using phenol/chloroform (1:1,
513 vol/vol). Protein enrichment at DNA regions was quantified using qPCR with the primers detailed in
514 **Supplementary Table 2.** Enrichment was determined by %Input method (%Input=2 ^ [CtInput-CtChIP] ×
515 IDF × 100%).

516 **Nuclear-Cytoplasmic Fractionation**

517 Nuclear fractionation was performed essentially as previously described with the following modifications
518 (*53*). Briefly, 0.5-1 g of Arabidopsis seedlings ground into fine powder in liquid nitrogen and then
519 homogenized in double the volume of pre-cooled (4 °C) lysis buffer (20 mM Tris-HCl, pH 7.4, 25% Glycerol,
520 20 mM KCl, 2 mM EDTA, 2.5 mM $MgCl_2$, 250 mM Sucrose and 5 mM DTT, add 1× protease inhibitor
521 cocktail (Roche) and 1× HALT-Phosphatase inhibitor added in fresh). The sample was filtered twice through
522 two layers of Mira cloth (Merck Millipore). The flow-through was spun 10 min at 2000 g, 4 °C. Supernatant,
523 consisting of the cytoplasmic fraction, was centrifuged 20 min at 13,000 g, 4 °C and collected. The pellet,
524 containing the nuclear fraction, was washed six times with 2.5 mL of nuclear resuspension buffer NRBT1
525 (20 mM Tris-HCl, pH 7.4, 25% Glycerol, 2.5 mM $MgCl_2$, 0.2% Triton X-100) and centrifuged 3 min at
526 1,500 g, 4 °C. The pellet was resuspended in 300 µL of pre-cooled NRBT2 (250 mM Sucrose, 10 mM Tris-
527 HCl, pH 7.5, 10 mM $MgCl_2$, 1% Triton X-100, 0.035% β-mercaptoethanol, and 1× protease inhibitor
528 cocktail added in fresh), and carefully overlaid on top of 300 µL NRBT3(1.7 M Sucrose, 10 mM Tris-HCl,
529 pH 7.5, 2 mM $MgCl_2$, 0.15% Triton X-100, 0.035% β-mercaptoethanol, and 1× protease inhibitor cocktail
530 added in fresh). These were centrifuged at 16,000 g for 55 min at 4 °C, and the final nuclear pellet was
531 resuspended in 2× SDS loading buffer. As quality controls for the fractionation, RbCL (Agrisera, AS03037,
532 1:3,000) protein was used as the cytoplasmic control, and histone H3 (Abcam, ab18521, 1:3,000) was used
533 as the nuclear control in immunoblot assays.

534 **Statistics and reproducibility**

535 All measurements were performed with three or more independent replicates from separate experiments.
536 The exact sample size and statistical test for each experiment are described in the relevant figure legends.
537 All results are presented as the means ± SEM. Statistical analyses were conducted using GraphPad Prism 10.

538 The Student's t test was used to assess statistical significance in Real-time q-PCR data. The other statistical
539 significance used One-way ANOVA test (α=0.05) with the Dunnett test and Two-way ANOVA (α=0.05) with
540 Tukey's HSD posthoc test. The Levels that are not significantly different are marked with the same letter.

541 **ACKNOWLEDGEMENTS**

542 This research was supported by University of Edinburgh Darwin Trust Scholarship awarded to MK. Z and
543 the Biotechnology and Biological Sciences Research Council (BB/N005147/1), and Leverhulme Trust

(RPG-2024-082) grants awarded to K.J.H. We thank Dr. Rist Van de Weyer who generated PIF7ox;*phyA-211* and first observed the PIF7ox hypocotyl phenotype in WLFR.

We thank Prof. Lin Li, Prof. Dr. Andreas Hiltbrunner, Dr. Gabriela Toledo-Ortiz and Dr. Mathias Zeidler who kindly shared *p35S::GFP-PIF7*, *p35S::PHYA-RFP*, *pPHYA::PHYA-sGFP* (NLS) and *fhy1-3;fhl-1* seeds.Thank Prof. Giltsu Choi for sharing *pif8-1;phyA-211*, *PIF8ox;phyA-211* and PIF8ox lines.

AUTHOR CONTRIBUTIONS

MK.Z and K.J.H. planned and designed the research. MK.Z conducted the experiments, which were analyzed by K.J.H. and MK.Z. A.R. generated the *pPIF7::PIF7-nanoLUC* line. The manuscript was prepared by MK.Z and K.J.H, subsequent editing performed by K.J.H and A.R.

REFERENCES

1 Liu, Y., Jafari, F. & Wang, H. Y. Integration of light and hormone signaling pathways in the regulation of plant shade avoidance syndrome. *Abiotech* **2**, 131-145 (2021). https://doi.org:10.1007/s42994-021-00038-1.

2 Franklin, K. A. Shade avoidance. *New Phytol* **179**, 930-944 (2008). https://doi.org:10.1111/j.1469-8137.2008.02507.x.

3 Prizeman-Green, P., Valdivia-Cabrera, M., Zhou, M., Grima, R. & Halliday, K.J. Arabidopsis thaliana phytochrome A sensory properties in canopy shade. *Proc Natl Acad Sci U S A* **123**, e2512201123 (2026). https://doi.org:10.1073/pnas.2512201123.

4 Mathews, S. & Sharrock, R. A. Phytochrome gene diversity. *Plant Cell Environ* **20**, 666-671 (1997). https://doi.org:10.1046/j.1365-3040.1997.d01-117.x.

5 Cheng, M. C., Kathare, P. K., Paik, I. & Huq, E. Phytochrome Signaling Networks. *Annu Rev Plant Biol* **72**, 217-244 (2021). https://doi.org:10.1146/annurev-arplant-080620-024221.

6 Du, J., Kim, K. & Chen, M. Distinguishing individual photobodies using Oligopaints reveals thermo-sensitive and -insensitive phytochrome B condensation at distinct subnuclear locations. *Nature Communications* **15** (2024). https://doi.org:10.1038/s41467-024-47789-1.

7 Casal, J. J., et al. Modes of action of phytochromes. Journal of Experimental Botany 49(319): 127-138 (1998). https://doi.org:10.1093/jexbot/49.319.127.

8 Rausenberger, J. *et al.* Photoconversion and Nuclear Trafficking Cycles Determine Phytochrome A's Response Profile to Far-Red Light. *Cell* **146**, 813-825 (2011). https://doi.org:10.1016/j.cell.2011.07.023. Hiltbrunner, A. *et al.* Nuclear accumulation of the phytochrome A photoreceptor requires FHY1. *Curr Biol* **15**, 2125-2130 (2005). https://doi.org:10.1016/j.cub.2005.10.042.

9 Genoud, T. *et al.* FHY1 Mediates Nuclear Import of the Light-Activated Phytochrome A Photoreceptor. *Plos Genet* **4** (2008). https://doi.org:10.1371/journal.pgen.1000143.

10 Li, J. G. *et al.* Transcription Factor ELONGATED HYPOCOTYL5 Plays a Role in the Feedback Regulation of Phytochrome A Signaling. *Plant Cell* **22**, 3634-3649 (2010). https://doi.org:10.1105/tpc.110.075788.

11 Pham, V. N., Kathare, P. K. & Huq, E. Phytochromes and Phytochrome Interacting Factors. *Plant Physiol* **176**, 1025-1038 (2018). https://doi.org:10.1104/pp.17.01384.

12 Jeong, J., Lee, Y. & Choi, G. Both phytochrome A and phyB interact with PHYTOCHROME-INTERACTING FACTORs through an evolutionary conserved phy(OPM)-APA interaction. *Nat Commun* **16**, 3946 (2025). https://doi.org:10.1038/s41467-025-59327-8.

13 Al-Sady, B., Ni, W., Kircher, S., Schafer, E. & Quail, P. H. Photoactivated phytochrome induces rapid PIF3 phosphorylation prior to proteasome-mediated degradation. *Mol Cell* **23**, 439-446 (2006). https://doi.org:10.1016/j.molcel.2006.06.011.

14 Oh, J., Park, E., Song, K., Bae, G. & Choi, G. PHYTOCHROME INTERACTING FACTOR8 Inhibits Phytochrome A-Mediated Far-Red Light Responses in Arabidopsis. *Plant Cell* **32**, 186-205 (2020).

https://doi.org:10.1105/tpc.19.00515.

15 Seaton, D. D. *et al.* Dawn and photoperiod sensing by phytochrome A. *P Natl Acad Sci USA* **115**, 10523-10528 (2018). https://doi.org:10.1073/pnas.1803398115.

16 Zhu, T., Yang, C., Xie, Y., Huang, S. & Li, L. Shade-induced lncRNA PUAR promotes shade response by repressing PHYA expression. *EMBO Rep* **24**, e56105 (2023). https://doi.org:10.15252/embr.202256105.

17 Leivar, P. *et al.* The Arabidopsis phytochrome-interacting factor PIF7, together with PIF3 and PIF4, regulates responses to prolonged red light by modulating phyB levels. *Plant Cell* **20**, 337-352 (2008). https://doi.org:10.1105/tpc.107.052142.

18 Xie, Y. *et al.* Phytochrome B inhibits the activity of phytochrome-interacting factor 7 involving phase separation. *Cell Rep* **42** (2023). https://doi.org:10.1016/j.celrep.2023.113562.

19 Huang, X. *et al.* Shade-induced nuclear localization of PIF7 is regulated by phosphorylation and 14-3-3 proteins in Arabidopsis. *Elife* **7** (2018). https://doi.org:10.7554/eLife.31636.

20 Park, E. *et al.* Phytochrome B inhibits binding of phytochrome-interacting factors to their target promoters. *Plant Journal* **72**, 537-546 (2012). https://doi.org:10.1111/j.1365-313X.2012.05114.x.

21 Martínez-García, J.F. *et al.* The Shade Avoidance Syndrome in Arabidopsis: The Antagonistic Role of Phytochrome A and B Differentiates Vegetation Proximity and Canopy Shade. *Plos One* **9**(2014). https://doi.org:10.1371/journal.pone.0109275.

22 Fraser, D. P. et al. Phytochrome A elevates plant circadian-clock components to suppress shade avoidance in deep-canopy shade. *Proc Natl Acad Sci U S A* (2021). https://doi.org:2010.1073/pnas.2108176118.

23 Mizuno, T., Oka, H., Yoshimura, F., Ishida, K. & Yamashino, T. Insight into the mechanism of end-of-day far-red light (EODFR)-induced shade avoidance responses in. *Biosci Biotech Bioch* **79**, 1987-1994 (2015). https://doi.org:10.1080/09168451.2015.1065171.

24 Burko, Y. et al. PIF7 is a master regulator of thermomorphogenesis in shade. *Nature Communications* **13** (2022). https://doi.org:10.1038/s41467-022-32585-6.

25 Ni, M., Tepperman, J. M. & Quail, P. H. PIF3, a phytochrome-interacting factor necessary for normal photoinduced signal transduction, is a novel basic helix-loop-helix protein. Cell 95, 657-667 (1998). https://doi.org:10.1016/S0092-8674(00)81636-0.

26 Lorrain, S., Trevisan, M., Pradervand, S. & Fankhauser, C. Phytochrome interacting factors 4 and 5 redundantly limit seedling de-etiolation in continuous far-red light. *Plant Journal* **60**, 449-461 (2009). https://doi.org:10.1111/j.1365-313X.2009.03971.x.

27 Sharrock, R. A. & Clack, T. Patterns of expression and normalized levels of the five Arabidopsis phytochromes. *Plant Physiol* **130**, 442-456 (2002). https://doi.org:10.1104/pp.005389.

28 Kim, L. *et al.* Light-induced nuclear import of phytochrome-A:GFP fusion proteins is differentially regulated in transgenic tobacco and. *Plant Journal* **22**, 125-133 (2000). https://doi.org:DOI 10.1046/j.1365-313x.2000.00729.x.

29 Toledo-Ortiz, G. *et al.* Subcellular sites of the signal transduction and degradation of phytochrome A. *Plant Cell Physiol* **51**, 1648-1660 (2010). https://doi.org:10.1093/pcp/pcq121.

30 Kevei, E., Schafer, E. & Nagy, F. Light-regulated nucleo-cytoplasmic partitioning of phytochromes. *J Exp Bot* **58**, 3113-3124 (2007). https://doi.org:10.1093/jxb/erm145.

31 Chen, F. *et al.* Phosphorylation of FAR-RED ELONGATED HYPOCOTYL1 is a key mechanism defining signaling dynamics of phytochrome A under red and far-red light in Arabidopsis. *Plant Cell* **24**, 1907-1920 (2012). https://doi.org:10.1105/tpc.112.097733.

32 Wang, H. & Deng, X. W. Arabidopsis FHY3 defines a key phytochrome A signaling component directly interacting with its homologous partner FAR1. *EMBO J* **21**, 1339-1349 (2002). https://doi.org:10.1093/emboj/21.6.1339.

33 Chen, F. *et al.* Phytochrome A Directly Targets Numerous Promoters for Individualized Modulation of Genes in a Wide Range of Pathways. *Plant Cell* **26**, 1949-1966 (2014). https://doi.org:10.1105/tpc.114.123950

34 Qu, G. P. *et al.* Reversible SUMOylation of FHY1 Regulates Phytochrome A Signaling in Arabidopsis. *Mol Plant* **13**, 879-893 (2020). https://doi.org:10.1016/j.molp.2020.04.002.

35 Menon, C., Klose, C. & Hiltbrunner, A. Arabidopsis FHY1 and FHY1-LIKE Are Not Required for Phytochrome A Signal Transduction in the Nucleus. *Plant Commun* **1**, 100007 (2020). https://doi.org:10.1016/j.xplc.2019.100007.

36 Al-Sady, B., Ni, W., Kircher, S., Schafer, E. & Quail, P. H. Photoactivated phytochrome induces rapid PIF3 phosphorylation prior to proteasome-mediated degradation. *Mol Cell* **23**, 439-446 (2006). https://doi.org:10.1016/j.molcel.2006.06.011.

37 Shen, H. *et al.* Light-induced phosphorylation and degradation of the negative regulator PHYTOCHROME-INTERACTING FACTOR1 from depend upon its direct physical interactions with photoactivated phytochromes. *Plant Cell* **20**, 1586-1602 (2008). https://doi.org:10.1105/tpc.108.060020.

38 Kim, C. *et al.* Phytochrome B photobodies are comprised of phytochrome B and its primary and secondary interacting proteins. *Nature Communications* **14** (2023). https://doi.org:10.1038/s41467-023-37421-z.

39 Hussain, E., Romanowski, A. & Halliday, K. J. PIF7 controls leaf cell proliferation through an AN3 substitution repression mechanism. *P Natl Acad Sci USA* **119** (2022). https://doi.org:10.1073/pnas.2115682119.

40 Hiltbrunner, A. *et al.* FHY1 and FHL act together to mediate nuclear accumulation of the phytochrome A photoreceptor. *Plant and Cell Physiology* **47**, 1023-1034 (2006). https://doi.org:10.1093/pcp/pcj087

41 Helizon, H. *et al.* Arabidopsis phytochrome A nuclear translocation is mediated by a far-red elongated hypocotyl 1-importin complex. *Plant Journal* **96**, 1255-1268 (2018). https://doi.org:10.1111/tpj.14107.

42 Willige, B. C. *et al.* PHYTOCHROME-INTERACTING FACTORs trigger environmentally responsive chromatin dynamics in plants. *Nat Genet* **53**, 955-+ (2021). https://doi.org:10.1038/s41588-021-00882-3

43 Du, J., Fan, D., He, J. & Chen, M. Twenty-Five Years of Photobodies: Formation, Composition, and the Two-Compartment Logic of Phytochrome B Signaling. *Plant Physiol* (2026). https://doi.org:10.1093/plphys/kiag058

44 Zhang, X. Y. *et al.* Liquid-liquid phase separation in diseases. *Medcomm* **5** (2024). https://doi.org:e64010.1002/mco2.640.

45 Leivar, P. *et al.* Multiple Phytochrome-Interacting bHLH Transcription Factors Repress Premature Seedling Photomorphogenesis in Darkness. *Curr Biol* **18**, 1815-1823 (2008). https://doi.org:10.1016/j.cub.2008.10.058.

46 Li, L. *et al.* Linking photoreceptor excitation to changes in plant architecture. *Genes Dev* **26**, 785-790 (2012). https://doi.org:10.1101/gad.187849.112.

47 Viczián, A. *et al.* Functional characterization of phytochrome interacting factor 3 for the circadian clockwork. *Plant and Cell Physiology* **46**, 1591-1602 (2005). https://doi.org:10.1093/pcp/pci175.

48 Andreou, A. I. & Nakayama, N. Mobius Assembly: A versatile Golden-Gate framework towards universal DNA assembly. Plos One 13 (2018). https://doi.org: 10.1371/journal.pone.0189892.

49 Urquiza-García, U. & Millar, A. J. Expanding the bioluminescent reporter toolkit for plant science with NanoLUC. Plant Methods 15 (2019). https://doi.org:10.1186/s13007-019-0454-4.

50 Zielinski, T., Moore, A. M., Troup, E., Halliday, K. J. & Millar, A. J. Strengths and Limitations of Period Estimation Methods for Circadian Data. *Plos One* **9** (2014). https://doi.org:10.1371/journal.pone.0096462

51 Wang, Z. S. *et al.* Proteasome-associated ubiquitin ligase relays target plant hormone-specific transcriptional activators. *Sci Adv* **8** (2022). https://doi.org:10.1126/sciadv.abn4466.

52 Zhang, S. M., et al. TANDEM ZINC-FINGER/PLUS3 Is a Key Component of Phytochrome A Signaling. Plant Cell 30(4): 835-852 (2018). https://doi.org: 10.1105/tpc.17.00677.

53 Rosler, J., Klein, I. & Zeidler, M. Arabidopsis *fhl/fhy1* double mutant reveals a distinct cytoplasmic action of phytochrome A. *P Natl Acad Sci USA* **104**, 10737-10742 (2007). https://doi.org:10.1073/pnas.0703855104.

54 Mancinelli, A.L. "[The physiology of phytochrome action]" in *Photomorphogenesis in Plants* (Springer, Dordrecht,1994).pp. 211-222. https://doi.org/10.1007/978-94-011-1884-2_10.

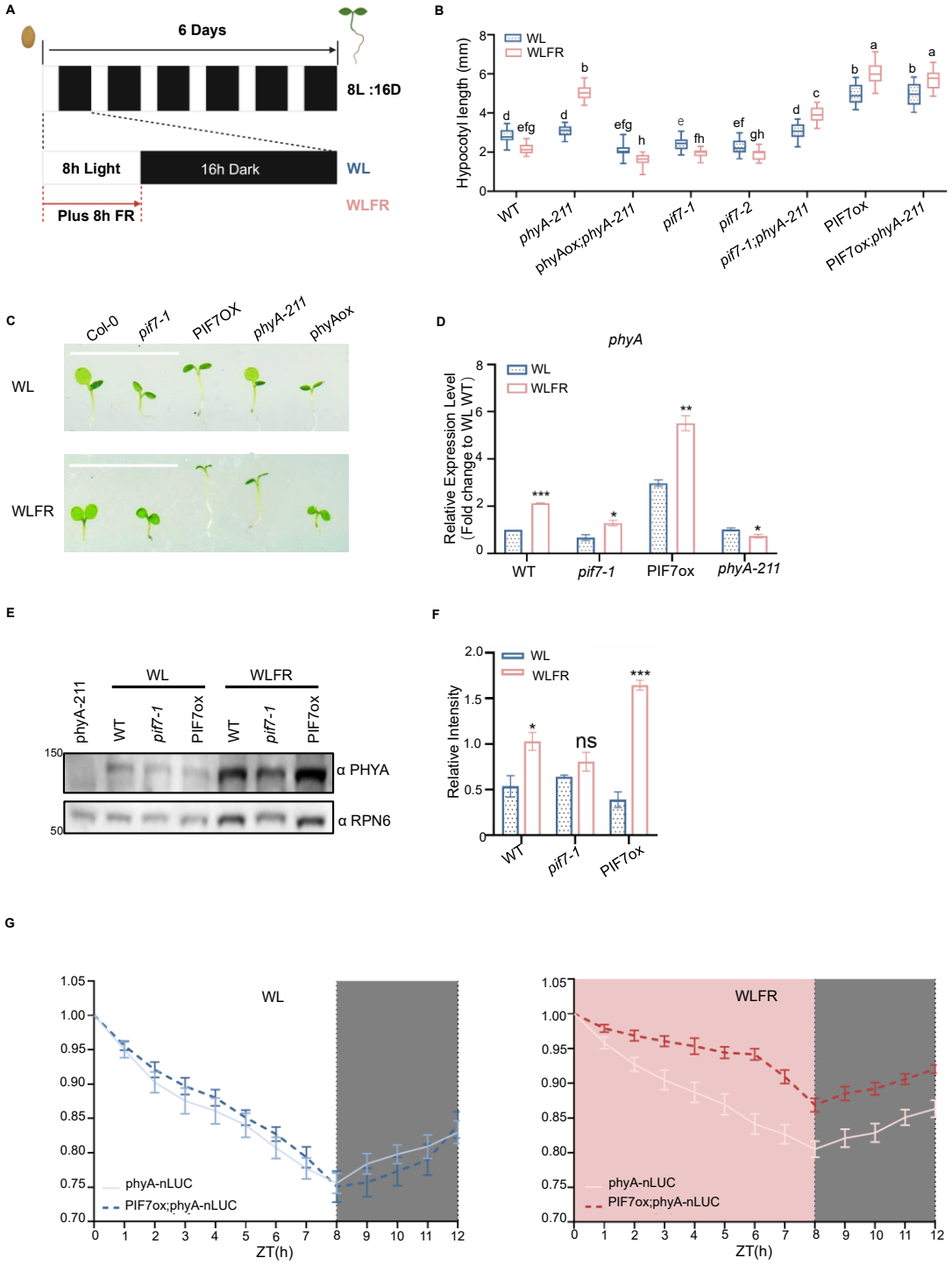
A
6 Days
8L :16D
8h Light
16h Dark
WL
WLFR
Plus 8h FR
B
WL
WLFR
Hypocotyl length (mm)
WT
phyA-211
phyAox;phyA-211
pif7-1
pif7-2
pif7-1;phyA-211
PIF7ox
PIF7ox;phyA-211
C
Col-0
pif7-1
PIF7OX
phyA-211
phyAox
WL
WLFR
D
phyA
WL
WLFR
Relative Expression Level (Fold change to WL WT)
WT
pif7-1
PIF7ox
phyA-211
E
phyA-211
WL
WLFR
WT
pif7-1
PIF7ox
α PHYA
α RPN6
F
WL
WLFR
Relative Intensity
ns
WT
pif7-1
PIF7ox
G
WL
WLFR
phyA-nLUC
PIF7ox;phyA-nLUC
ZT(h)

Fig. 1. PIF7ox moderates phyA function under WLFR.

(**A**) Schematic of experimental growth conditions. Seeds were sown on 1/2 MS plates and exposed to 4 hours (h) of light to induce germination, followed by 20 h of dark. Seedlings were then grown for 6 days in white light (WL) photoperiods with or without supplementary far-red (WLFR), lowering the R:FR to 0.20 (red arrow). All experiments were conducted at 22 °C under a photosynthetically active radiation (PAR) fluence rate of 85 ± 5 µmol m^{-2} s^{-1}. (**B**) Hypocotyl length (mm) of WT (Col-0), *phyA-211*, *p35S::PHYA-tagRFP:terRbcS;phyA-211* (phyAox), *pif7-1*, *pif7-2*, *pif7-1;phyA-211*, *p35S::PIF7ox-FLASH* (PIF7ox) and PIF7ox*;phyA-211*. Seedlings were grown for 6 days in WL or WLFR. (**C**) Representative images of WT (Col-0), *pif7-1*, PIF7ox, phyAox and *phyA-211* seedlings grown in WL or WLFR for 6 days. Scale bar = 1 cm.
(**D**) Real-time qPCR was used to quantify *PHYA* mRNA levels in WT (Col-0), *pif7-1*, PIF7ox and *phyA-211* seedlings using *PP2A* as the internal control. Samples were collected at ZT7 (1 hour before dusk) from 6d-old seedlings grown in WL or WLFR. (**E** and **F**) PHYA protein levels in WT (Col-0), *pif7-1* and PIF7ox were determined by immunoblotting. Anti-PHYA was used to detect native phyA, while anti-RPN6 served as an internal control. The bar chart (**F**) displays the relative levels of phyA, normalised to RPN6, based on data from four biological replicates collected at ZT7. (**G**) Diel phyA-nLUC levels were quantified in WT (Col-0), *pif7-1* and PIF7ox lines. The phyA-nLUC line was generated by expressing (p*PHYA::PHYA-nLUC*) in *phyA-211*, while the PIF7ox;phyA-nLUC was generated by introgressing *pPHYA::PHYA-nLUC* into the PIF7ox line. Bioluminescence signals were recorded from day 6.
For (**B**, **D**, **F** and **G**) data are presented as mean values ± s.e.m., for n=25 (seedling numbers) in (B); and for n=3,4 and 9 biological repeats in (**D**, **F** and **G**), respectively. For (**B**) a Two-way ANOVA was conducted to assess statistical significance across light conditions for each genotype (α=0.05), followed by Tukey's HSD post hoc test for pairwise multiple comparisons. Groups that do not differ significantly are indicated by the same letter. For (**D** and **F**) Asterisks indicate significant differences from the WL values (*, $P < 0.05$; **, $P < 0.01$; and ***, $P < 0.001$; Student's t test).

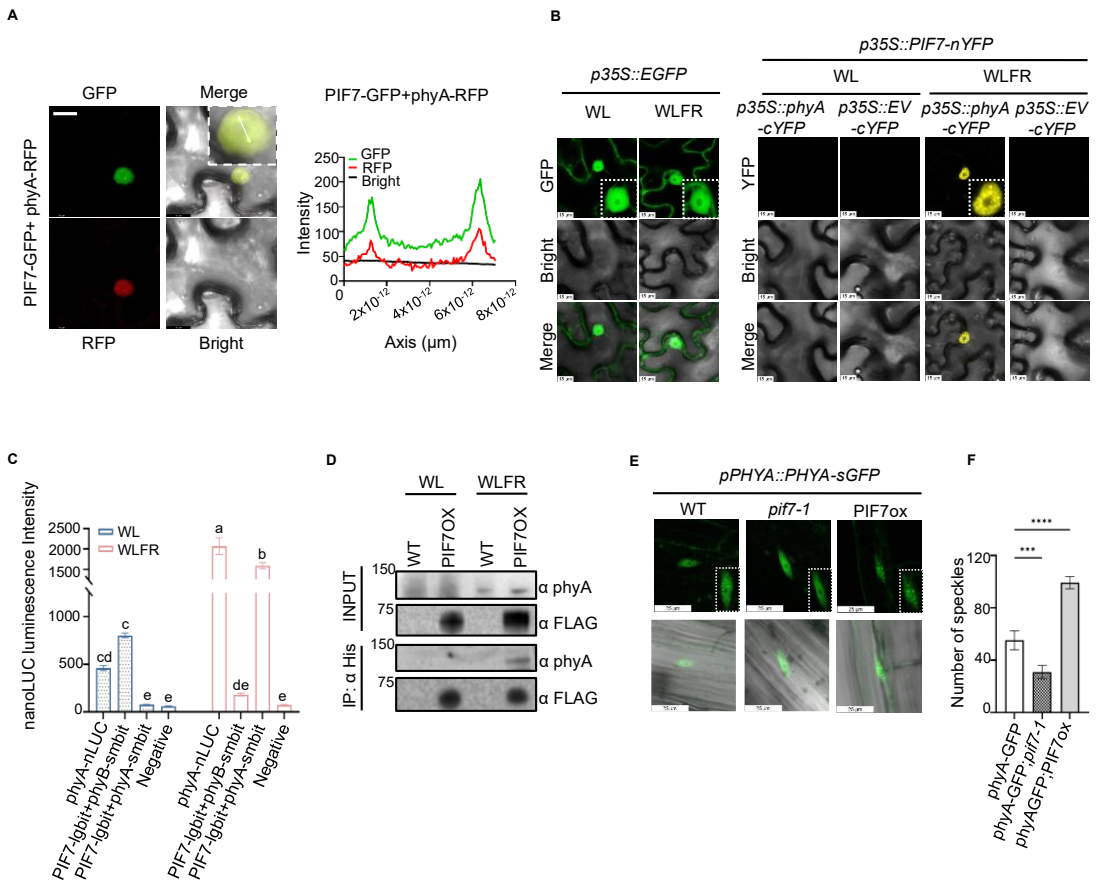

Fig. 2. In WLFR PIF7 and phyA interact in nuclear photobodies.

(**A**) Subcellular localization of *p35S::PIF7-sfGFP* (PIF7-GFP) and *p35S::PHYA-RFP* (phyA-RFP) under WLFR in *Nicotiana benthamiana* leaf epidermal cells. Co-localisation is evident from the chart (right) which traces the GFP and RFP channel signals along the white bar (intersecting two photobodies) shown in merged nucleus image (left). (**B**) Bimolecular Fluorescence Complementation (BiFC) assays confirm PIF7 and phyA interact in nuclear photobodies. BiFC was detected between *p35S::PIF7-nYFP* (PIF7-nYFP) and *p35S::PHYA*-cYFP (phyA-cYFP) in WLFR, but not with the *p35S::EV-cYFP* (EV-cYFP, empty vector) control. The *p35S::EGFP,* the transformation control, was located across cellular compartments irrespective of light conditions. All the constructs were expressed in *N. benthamiana.* Scale Bar =15μm. (**C**) Split NanoLUC (nLUC) assay demonstrates PIF7 and phyA physically interact. *p35S::*PIF7-lgbitnLUC (PIF7-lgbit), *p35S::PHYA-smbitnLUC* (phyA-smbit), *p35S::PHY*B-smbitnLUC (phyB-smbit) and *p35S::PHY*A-nLUC (phyA-nLUC) reporter constructs were expressed in *Nicotiana benthamiana*. A WLFR-dependent interaction was demonstrated for PIF7-lgbit+phyA-smbit. PhyA-nLUC was used as light conditional controls, and phyB-smbit+phyA-smbit as the negative control. (**D**) *In vivo* co-immunoprecipitation assay (Co-IP) illustrates that under WLFR, phyA interacts with PIF7 in Arabidopsis. Anti-His beads were used to pull down PIF7 from PIF7ox (*p35S::PIF7-FLASH*; 9×Myc-6×His-3×FLAG) or the WT(*Col-0*) negative control. Anti-PHYA and anti-FLAG used for detecting phyA and PIF7 respectively, in the IP/Input. Samples were collected at ZT7 from 6-d old seedlings exposed to WL or WLFR. (**E** and **F**) PIF7 involvement in PHYA photobody formation was assessed by expressing *pPHYA::PHYA-sGFP* (PHYA-GFP) in *pif7-1* and *PIF7ox* backgrounds. Representative images of hypocotyl epidermal cell nuclei are shown (E), together with quantification of nuclear photobodies from

10 nuclei per seedling across five seedlings (F). Data are presented as mean ± s.e.m. Images were captured at ZT7 after 6 days of growth under WL or WLFR. Imaging focused on the mid-hypocotyl region using a 20 × 9.91 objective lens. Scale bar = 25 μm.

For **(A**, **B**, **E** and **F**), the GFP/YFP and RFP are specific channels with associated filters, signals were detected using 488nm and 552nm laser wavelengths, the Bright is bright field. For **(C**) data are presented as mean values ± s.e.m., n=12 (leaf numbers). A Two-way ANOVA was conducted to assess statistical significance across light conditions for each genotype (α=0.05), followed by Tukey's HSD post hoc test for pairwise multiple comparisons. Groups that do not differ significantly are indicated by the same letter. For (**F**) A One-way ANOVA test was used to obtain statistical significance (α=0.05); the Dunnett test for multiple comparisons. Asterisks indicate significant differences from the phyA-GFP values (***, $P < 0.001$; and ****, $P < 0.0001$).

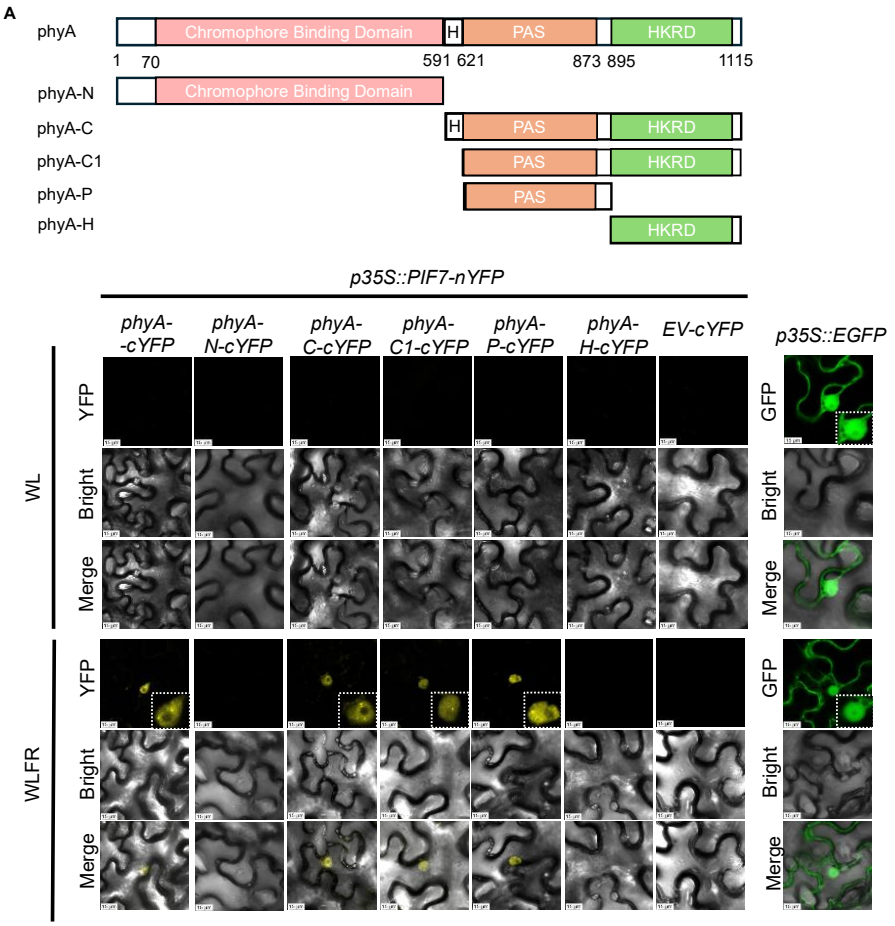
A
phyA
Chromophore Binding Domain
H
PAS
HKRD
1
70
591
621
873
895
1115
phyA-N
phyA-C
phyA-C1
phyA-P
phyA-H
p35S::PIF7-nYFP
phyA-cYFP
phyA-N-cYFP
phyA-C-cYFP
phyA-C1-cYFP
phyA-P-cYFP
phyA-H-cYFP
EV-cYFP
p35S::EGFP
WL
WLFR
YFP
Bright
Merge
GFP

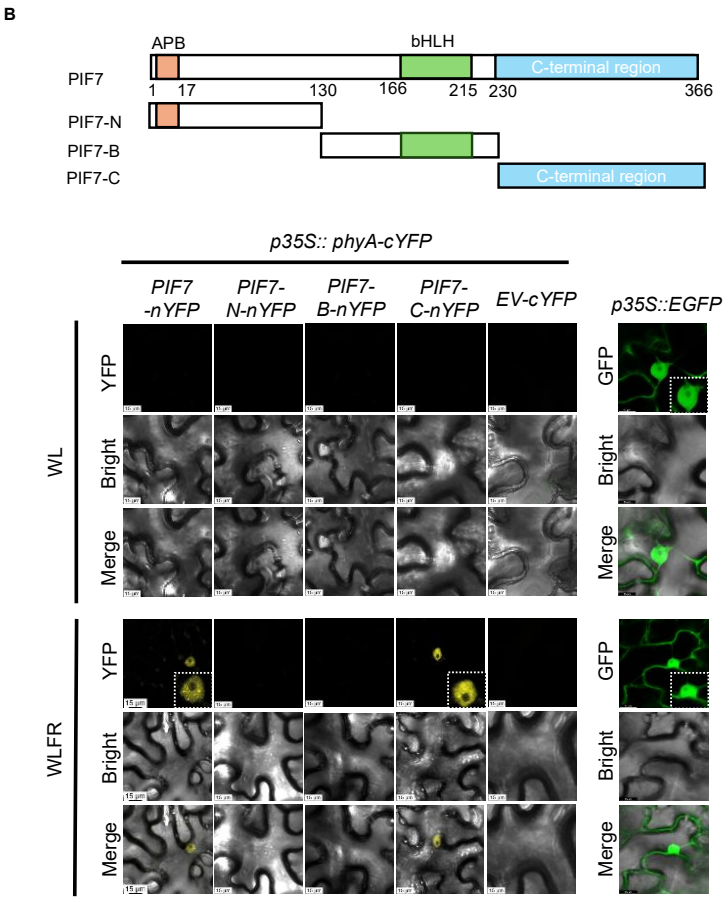
B
APB
bHLH
C-terminal region
PIF7
1
17
130
166
215
230
366
PIF7-N
PIF7-B
PIF7-C
p35S:: phyA-cYFP
PIF7-nYFP
PIF7-N-nYFP
PIF7-B-nYFP
PIF7-C-nYFP
EV-cYFP
p35S::EGFP
WL
WLFR
YFP
Bright
Merge
GFP

Fig. 3. The PIF7-phyA Interaction Depends on the PIF7 C-terminal Region.

(A and **B)** BIFC assays using truncated constructs identify the PHYA PAS domain and the PIF7 C-terminal Region, as important for the phyA-PIF7 interaction. The construct diagrams depict the complete and truncated PHYA and PIF7 protein structures. Full-length and truncated variants were fused to C-terminal nYFP (PIF7) or cYFP (PHYA) to generate BiFC constructs. The *p35S::EGFP* construct served as a transformation control. PIF7-nYFP + phyA-cYFP was used as a positive control, whereas PIF7-nYFP + *p35S::EV-cYFP* and phyA-cYFP + *p35S::EV-nYFP* served as negative controls. All constructs were transiently expressed in *Nicotiana benthamiana* leaf epidermal cells. 488nm lasers were used to detect the YFP/GFP signals. Representative images from three independent replicates are shown. Scale Bar=15μm.

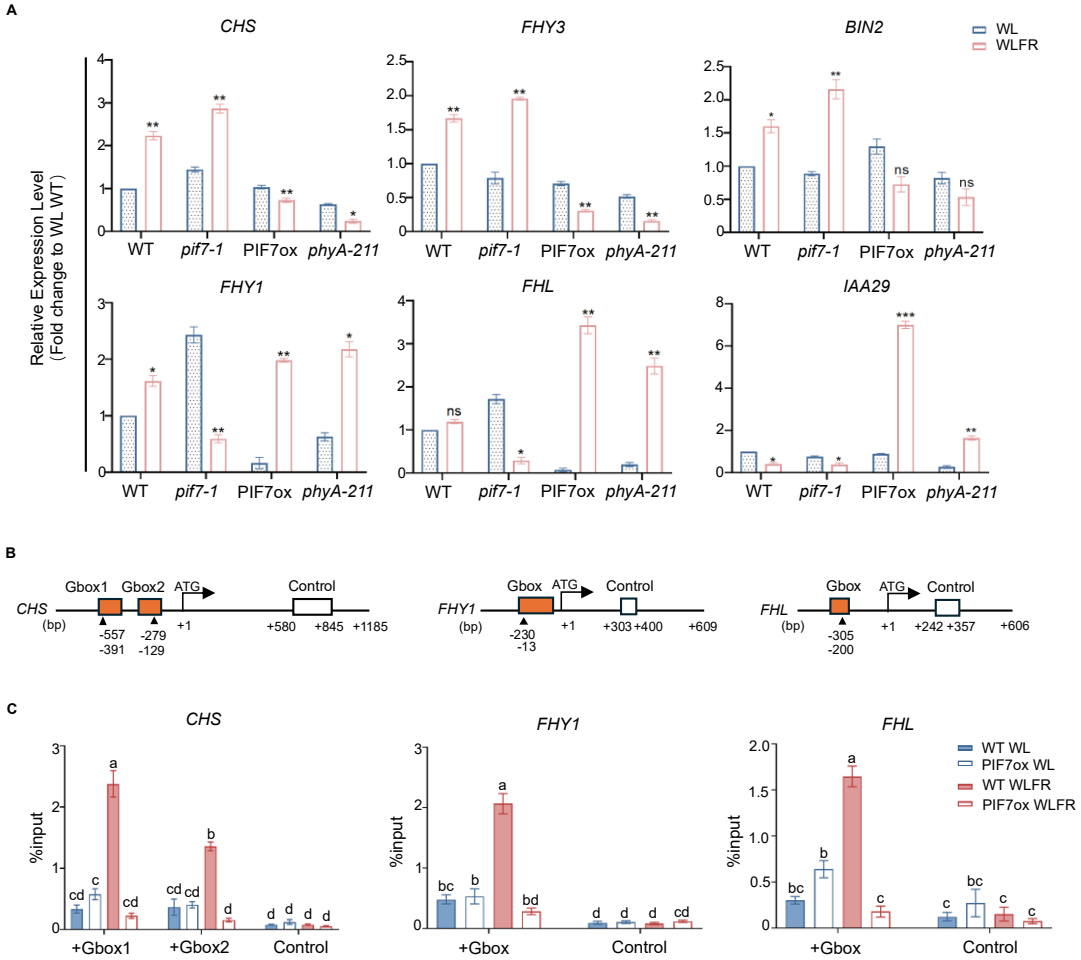

Fig. 4. PIF7 inhibits phyA-mediated regulation of target genes.

(**A**) Real-time qPCR analysis of *CHS, FHY3, BIN2, FHY1, FHL* and *IAA29* expression in WT (*Col-0*), *pif7-1*, PIF7ox and *phyA-211*. Transcript levels were normalised to the *PP2A* internal control. (**B**) Schematics representations of the *CHS*, *FHY1* and *FHL* gene and promoter regions The orange boxes indicate primer target regions encompassing G-box elements, while the white boxes denote exon regions used as assay controls. Arrows indicate base pair (bp) position. (**C**) Chromatin immunoprecipitation (ChIP)-qPCR illustrates PIF7ox reduces phyA enrichment at *CHS, FHY1,* and *FHL* promoters under WLFR. Assays were conducted WT (*Col-0*) or PIF7ox seedlings sampled at ZT7 on day 6. Native phyA was immobilised on protein A/G beads using an anti-phyA antibody, and promoter enrichment quantified by Real-time qPCR at G-box promoter regions and coding regions, which served as negative controls. Data shown is normalised to input samples.

For (**A** and **C**) data are presented as mean values ± s.e.m., *n*=3 (biological repeats). For (**A**) a Student's t-test was used to assess statistical significance between the WL/WLFR for each genotype, asterisks indicate significant differences from the WL values (*, $P < 0.05$; **, $P < 0.01$; and ***, $P < 0.001$). For (**B**) a Two-way ANOVA was conducted to assess statistical significance across light conditions for each genotype (α=0.05), followed by Tukey's HSD post hoc test for pairwise multiple comparisons. Groups that do not differ significantly are indicated by the same letter.

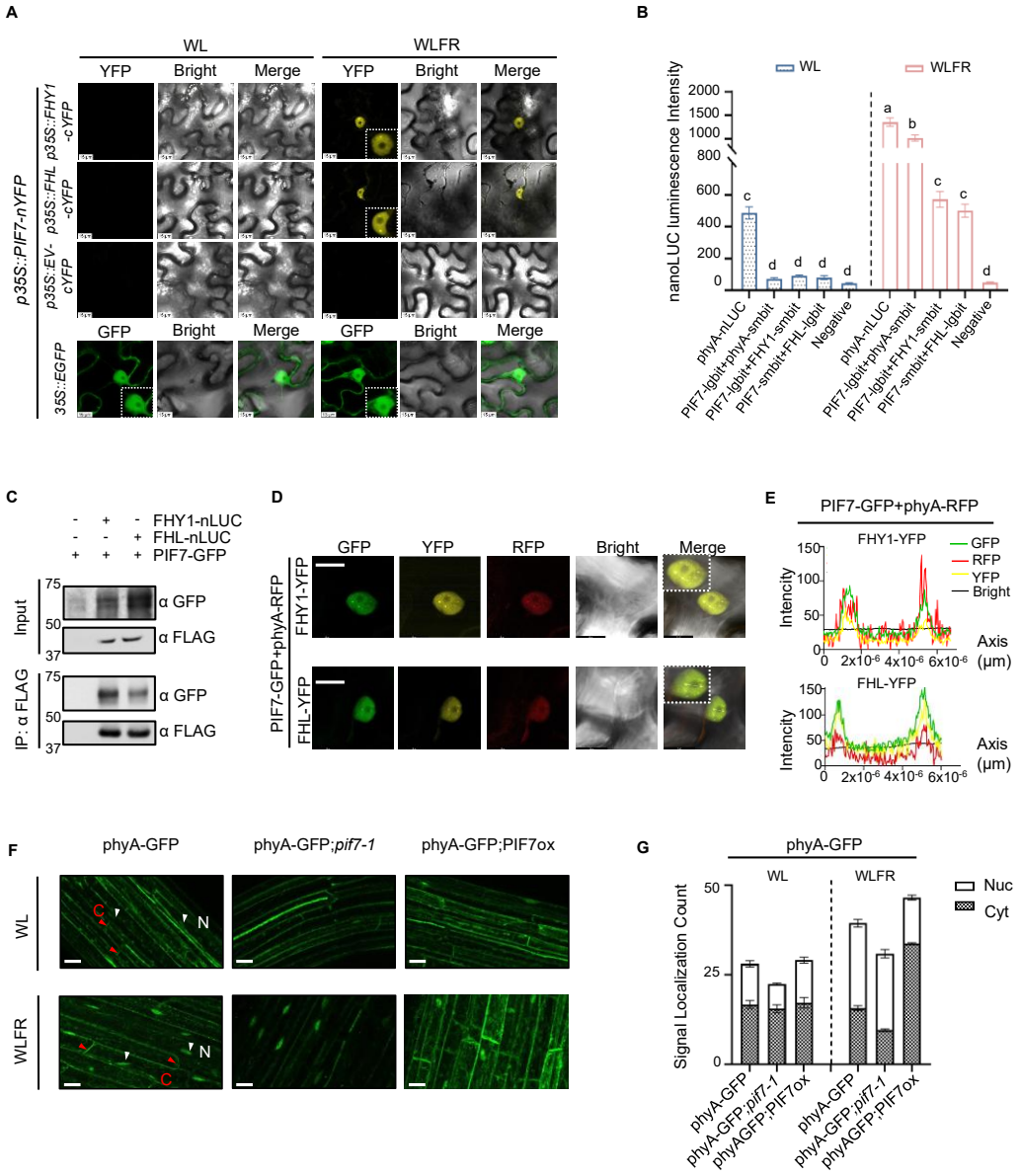

Fig. 5. PIF7 interacts with FHY1/FHL in WLFR.

(**A**) The BiFC assay illustrates that PIF7 interacts with FHY1 and FHL in WLFR. Interaction fluorescence was detected when *p35S::FHY1-cYFP* (FHY1-cYFP) or *p35S::FHL-cYFP* (FHL-cYFP) were co-expressed with *p35S::PIF7-nYFP* (PIF7-nYFP) in *N. benthamiana* under WLFR. The *p35S::EGFP* used as the transformation control. (**B**) Interactions between PIF7 and FHY1/FHL using a split NanoLUC complementation assay under WL and WLFR. Bioluminescence signals were detected upon co-expression of *p35S::PIF7-lgbitnLUC* (PIF7-lgbit) and *p35S::FHY1-smbitnLUC* (FHY1-smbit) or *p35S::PIF7-smbitnLUC* (PIF7smbit) and *p35S::FHL-lgbitnLUC* (FHL-lgbit) in the transient *N. benthamiana* expression system. The phyA-nLUC and PIF7-lgbit + phyA-smbit served as positive controls in WLFR, whereas PIF7-smbit + phyA-smbit was used as a negative control in WLFR. (**C**) Immunoprecipitation assay demonstrating PIF7 interacts with FHY1/FHL *in vivo* under WLFR. *p35S::FHY1/FHL-nanoLUC × 3FLAG × 10His* (FHY1-nLUC) and *p35S::PIF7-sfGFP* (PIF7-GFP) constructs were transiently expressed in *N. benthamiana* leaves. Anti-FLAG beads were used to pull

down FHY1/FHL and its target proteins by Co-IP, while anti GFP antibodies were used to detect PIF7-GFP. (**D** and **E**) Fluorescence assays showing PIF7, phyA and FHY1/FHL co-localise in nuclei and photobodies. *p35S::PIF7-sfGFP* (PIF7-GFP), *p35S::FHY1-YFP* (FHY1-YFP) and *p35S::FHL-YFP* (FHL-YFP), and *p35S::PHYA-RFP* (phyA-RFP) constructs were transiently expressed in *N. benthamiana* leaves. The merged image (D) signifies co-localisation in epidermal cell nuclei, and (E) displays GFP, YFP and RFP channel signals along the white line transect shown in the merged nuclear image. (**F**) Fluorescence imaging to assess the effect of PIF7 on phyA-GFP cellular distribution under WL and WLFR. Lines of phyA-GFP;*pif7-1* and phyA-GFP;PIF7ox were generated by introgressing *pPHYA::PHYA-sGFP* into *pif7-1* and PIF7ox. Images were captured at ZT7 after 6 days of WL or WLFR. The images were collected from mid-hypocotyl region using a 20 × 9.91 objective lens. The white arrows and N label indicate nuclear, while red arrows and C label indicate cytosolic signals. Scale bar = 25 µm. (**G**) Quantification of nuclear vs cytosolic signals from hypocotyl epidermal cells of phyA-GFP, phyA-GFP;*pif7-1* and phyA-GFP;PIF7ox. A total 50 cells were counted in each of 6 biological repeats.

For (**G**, **D** and **F**) 488nm and 552nm lasers were used for detecting GFP/YFP and RFP signals. Scale bar=15µm. For (**B** and **G**) data are presented as mean values ± s.e.m., n=12 (leaf numbers) in (**B**) and n=6 (biological repeats) in (**G**). In (**B**) a Two-way ANOVA was conducted to assess statistical significance across light conditions for each genotype (α=0.05), followed by Tukey's HSD post hoc test for pairwise multiple comparisons. Groups that do not differ significantly are indicated by the same letter.

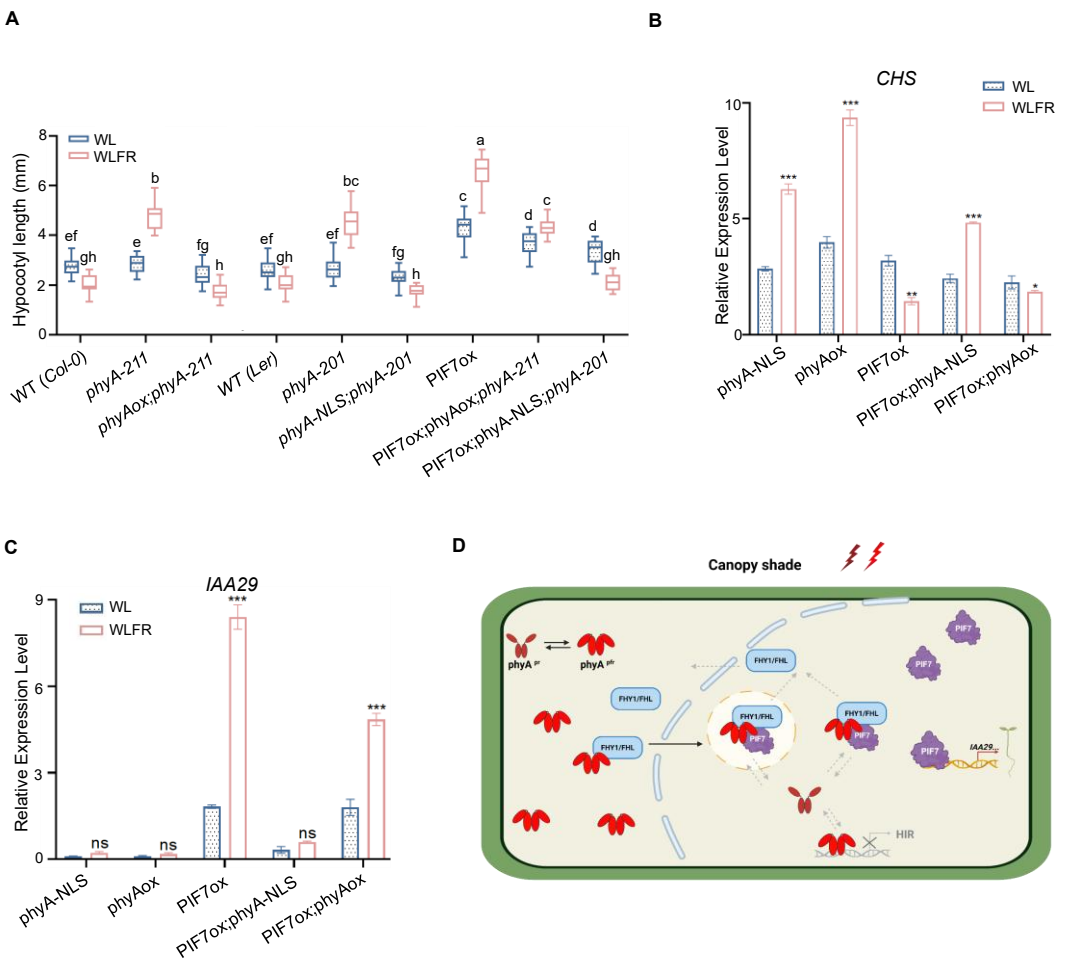

Fig. 6. PIF7 cannot suppress phyA-NLS action.

(**A**) Hypocotyl length (mm) of 6d-old WT (Col-0), *phyA-211, phyAox;phyA-211,* WT (Ler), *phyA-201, phyA-NLS;phyA-201*, PIF7ox, PIF7ox*; phyAox;phyA-211,* and PIF7ox*;phyA-NLS;phyA-201* seedlings grown in WL or WLFR. Double and triple mutant lines were generated through genetic crossing. (**B** and **C**) phyA-NLS restores phyA control of *CHS* and *IAA29* in PIF7ox seedlings not phyAox. Relative expression of *CHS* and *IAA29* compared to *PP2A* internal control in phyA-NLS*;phyA-201*, (phyA-NLS), phyAox, PIF7ox and PIF7ox;phyA-NLS*;phyA-201* (PIF7ox;phyA-NLS). Samples were collected at ZT7 on day 6 from seedlings grown in WL or WLFR.(**D**) Schematic depicting the cellular model for PIF7 control of phyA action under canopy shade. In persistent shade conditions phyA is transported to the nucleus by the FHL/FHY1 transporters. PIF7 also accumulates in the nucleus, where it interacts with phyA and with FHL/FHY1 to form photobodies. Here PIF7 exerts a dual effect on phyA by limiting its nuclear translocation and repressing phyA-mediated regulation of target gene expression. Consequently, PIF7 is able to amplify SAS-mediated hypocotyl elongation by blocking the antagonistic action of phyA. The image created in BioRender (https://BioRender.com).

For (**A**-**C**), data are presented as mean values ± s.e.m., *n*=24 (seedling numbers) in **a**. *n*=3 (biological repeats) in (**B**) and (**C**). For (**A**) a Two-way ANOVA was conducted to assess statistical significance across light conditions for each genotype (α=0.05), followed by Tukey's HSD post hoc test for pairwise multiple comparisons. Groups that do not differ significantly are indicated by the same letter. For (**B** and

C) **a** Student's t test was used to assess statistical significance between the WL/WLFR for each genotype, asterisks indicate significant differences from the WL values (*, $P < 0.05$; **, $P < 0.01$; ***, $P < 0.001$).